A review on thermally induced phase separation technology in the fabrication of microporous polymer membrane devices for sustained-repellent delivery: Crystallization and morpholog…

Article · August 2024

DOI: 10.1002/pol.20240232

5 authors, including:

Antonio Benjamim Mapossa
The University of Calgary
40 PUBLICATIONS **513** CITATIONS
SEE PROFILE

Robert Tewo
13 PUBLICATIONS **91** CITATIONS
SEE PROFILE

Suprakas Sinha Ray
Council for Scientific and Industrial Research, South Africa
849 PUBLICATIONS **33,992** CITATIONS
SEE PROFILE

Uttandaraman Sundararaj
The University of Calgary
426 PUBLICATIONS **16,725** CITATIONS
SEE PROFILE

Received: 23 March 2024 | Revised: 27 July 2024 | Accepted: 4 August 2024

DOI: 10.1002/pol.20240232

REVIEW

JOURNAL OF POLYMER SCIENCE WILEY

A review on thermally induced phase separation technology in the fabrication of microporous polymer membrane devices for sustained-repellent delivery: Crystallization and morphological studies

António Benjamim Mapossa[1,2] | **Robert Kimutai Tewo**[3] | **Suprakas Sinha Ray**[4,5] | **Washington Mhike**[6] | **Uttandaraman Sundararaj**[1]

[1]Department of Chemical and Petroleum Engineering, University of Calgary, Calgary, Alberta, Canada

[2]Department of Chemical Engineering, Institute of Applied Materials, University of Pretoria, Pretoria, South Africa

[3]Department of Chemical Engineering, Dedan Kimathi University of Technology, Dedan Kimathi, Kenya

[4]Centre for Nanostructures and Advanced Materials, DSI-CSIR Nanotechnology Innovation Centre, Council for Scientific and Industrial Research, Pretoria, South Africa

[5]Department of Chemical Sciences, University of Johannesburg, Johannesburg, South Africa

[6]Polymer Technology Division, Department of Chemical, Metallurgical and Materials Engineering, Tshwane University of Technology, Pretoria, South Africa

Correspondence
Suprakas Sinha Ray, Centre for Nanostructures and Advanced Materials, DSI-CSIR Nanotechnology Innovation Centre, Council for Scientific and Industrial Research, Pretoria 0001, South Africa.
Email: rsuprakas@csir.co.za

Uttandaraman Sundararaj, Department of Chemical and Petroleum Engineering, University of Calgary, Calgary, AB T2N 1N4, Canada.
Email: ut@ucalgary.ca

Funding information
Natural Sciences and Engineering Research Council of Canada (NSERC), Grant/Award Number: 05503/2020; Nanotechnology Innovation Centre, Grant/Award Number: C6ACH77; Council for Scientific and Industrial Research, Grant/Award Number: C6A0059

Abstract

This article reports recent advances in thermally induced phase separation technology in fabricating microporous scaffold polymeric membranes as devices suitable for the controlled release of insect repellent. The key aspects, such as the crystallization behavior and morphological study of the polymeric membrane-based repellent, were reported and discussed. Studies demonstrated that trapping of such repellents into microporous polymeric materials can be achieved by spinodal decomposition of the polymer/liquid repellent system. Usually, solubility is enhanced at elevated temperatures. Rapid cooling of such solution below the UCST leads to the formation of cocontinuous phase structures by decomposition. The polymer then forms an open-cell structure with the repellent trapped inside. Approaches to forming such an open-cell polymer structure containing mosquito repellent were successfully performed and confirmed with the SEM and POM techniques. It showed the structure of a polymer and liquid repellent prepared by spinodal decomposition, providing proof that thermally induced spinodal decomposition is a route to trap liquid mosquito repellent into a microporous polymer matrix. Additionally, the effects of polymer type, repellent nature, cooling conditions, and fillers on the morphology and performance of TIPS membranes are also discussed. Finally,

challenges in developing microporous polymeric membrane-based repellent using TIPS technology are addressed.

KEYWORDS

crystallization and morphology, microporous, polymer, repellent, TIPS method

1 | INTRODUCTION

Microporous polymer development and its application in biomedical/tissue engineering through the making of scaffolds, such as filtration membranes or liquid reservoirs, have gained great interest in recent times.[1,2] The most popular and efficient technique that has been employed to produce microporous polymer materials is thermally induced phase separation (TIPS).[3–5] TIPS is a phase separation method for liquid–liquid (L–L) and solid–liquid (S–L) phases with the capacity to precisely control the release of active substances and create complex porous structures.[6,7] During the TIPS procedure, a polymer substance /blend is heated to a sufficiently high temperature to allow melt-blending of the components into a homogenous phase.[6,7] Typically, the diluent is a high boiling point, low molecular weight solvent that dissolves polymers at higher temperatures but not at room temperature.[4,7] In general, TIPS occurs based on the following steps: (i) a high-boiling, low molecular weight liquid or solid diluent is melt-blended with the polymer to create a homogenous polymer/diluent solution at a high temperature; (ii) the polymer/diluent mixture is molded into the required shape, such as tubes, hollow fibers, or flat sheets; (iii), phase separation occurs through solution cooling to cause thermal energy removal and solidification of the polymer, and (iv) a microporous structure is created by solvent extraction, which eliminates the diluent.[8,9]

In the fabrication of microporous polymer systems via TIPS, when the homogenous solution is cooled, phase separation is induced, leading to either an L–L or S–L phase separation that creates two liquid phases, that is, a solvent-rich and a polymer-rich phase.[10] The temperature at which the L–L phase separation occurs depends on the concentration ratio and the chemistry of the polymer and the solvent.[11] In microporous polymer systems, the phase separations thermodynamics and kinetics govern the membrane shape developed.[6,8] Crystalline polymers undergo an L–L phase separation followed by polymer crystallization, and in the case of S–L phase separation, a spherulitic membrane structure is formed.[12] The crystallization-free enthalpy of the mixture solution also contributes to phase separation in the development of microporous materials; when a solution undergoes spinodal decomposition during a thermodynamically unstable state, the liquid–liquid phase separation happens spontaneously.[13] L–L phase separation occurs when a solution is cooled below the spinodal phase transition line, and remixing occurs when it is heated. Crystal nuclei formation in S–L phase separation conversely requires high supercooling; hence, the melting and crystallization temperatures during cooling and successive heating tend to be different.[9] Nucleation and growth mechanisms in microporous structure development are linked to the cooling rate dependence. Polymer solution demixing behavior can be obtained via the changes in its optical appearance or cloud-point observations.[6] However, instantaneous demixing mechanism information cannot be obtained via cloud point measurements, but an alternative method used is differential scanning calorimetry (DSC).[13,14] In polymer systems, DSC can track change in latent heat/enthalpy, giving a better understanding of the phase separation of polymer solutions compared with cloud point measurements. Recently, hot-stage polarized-light microscopy has also been employed to describe the S–L separation induced by crystallization due to cooling-rate dependence in visualizing the crystals.

Motivated by the previous reviews published conducted by (i) Ma et al.,[15] where they reported the development of polymeric membranes by TIPS method by going over the membrane materials, effective preparation parameters, mass transfer's role in the TIPS method, modeling the membrane fabrication process, and the use of TIPS membranes; (ii) Tang et al.[10] provided a comprehensive review of the creation, research, and manufacturing of PVDF microporous membranes using TIPS for use in water treatment applications involving microfiltration and ultrafiltration (MF/UF); and (iii) Liu et al.[8] summarized the investigation of various microporous polymeric membranes made using the TIPS technique, where they focused on the relationships between the membrane structures and the polymer/diluent system thermodynamics, the kinetics of crystallization and phase separation, herein this current review discusses TIPS technology for polymer devices based repellent productions to combat against Malaria. It still remains the principal cause of hospital consultations in tropical and subtropical endemic regions, particularly in sub-Sahara Africa, which contributes to the high number of mortalities.[16] According to the latest World Health Organization (WHO) report, in 2021,

approximately 247 million malaria cases were reported, with an estimated number of 61,900 mortalities.[16] Most of the reported cases include children younger than 5 years and pregnant women who are considered most susceptible to malaria.[16,17] During that year, the WHO reported that approximately 76% of the total number of fatalities were children.[17] Therefore, to develop polymer based-insect repellent devices using TIPS technology for safe personal protection against mosquito bites is required and mandatory.

The reviews previously mentioned demonstrated success in the fabrication of microporous membranes using various diluents, such as mineral oil, diphenyl ether, liquid paraffin, decalin, diisodecyl phthalate, dodecanol/soybean oil (SBO), isoparaffin, soybean oil, and dioctyl phthalate. However, to the best of our knowledge, a review of TIPS technology in the fabrication of microporous polymer membrane devices for slow repellent-delivery, with highlights on the crystallization and morphological studies, has not yet been explored, which is therefore endeavored here. It is important to note that this work focuses on the recent advances in the use of insect liquid repellents as diluents to fabricate microporous polymeric membranes for medical applications. Furthermore, studies on crystal growth theories and the behavior of supercooled liquids to interpret the morphology in terms of the independent variable's crystallization temperature and polymer and repellent fraction need to be further explored. This has also served as the foundation for the present research to critically examine the crystallization and morphological studies of TIPS technology in fabricating microporous polymer membranes as devices for slow-repellent delivery.

Finally, the information centralized in this work will help readers learn more about this challenging field and will be a useful reference in the future. Understanding the procedure of preparation of microporous polymer by TIPS technology as well the structure–function relationship of the polymer and insect repellent is the key to the effective design of a repellent delivery polymeric devices to be used for slow-release rate of repellents and prolonging the period of protection of people against mosquito bites, reducing malaria transmission in endemic regions, such as in Sub-Saharan Africa.

2 | OVERVIEW OF THE MICROPOROUS POLYMER MEMBRANE FABRICATION

Various methods, such as inversion phase, melt extrusion, controlled stretching, and electrospinning, can be used to prepare microporous polymeric membranes depending on the desired membrane morphology.[18,19] To choose the best methods of preparing polymer scaffolds, its application is a key requirement.[20–22] Nowadays, the inversion phase method, also called phase separation, is widely used due to its scalability and versatility. Phase inversion is a demixing procedure that yields a solid membrane by the first phase-separating a polymer dope solution into polymer-rich and polymer-lean phases, then removing the solvent.[23] Up to now, four principal types of phase inversion techniques have been employed to fabricate microporous polymer structures with interconnected open-cell porous networks. These include solvent-induced phase separation (SIPS), nonsolvent-induced phase separation (NIPS), TIPS,[15] and thermally assisted evaporation phase separation (TAEPS).[24] Below in the next sections, the TIPS method is carefully reported and described. This is because this work investigates the literature studies based on the fabrication of microporous polymer membranes as devices for repellent using the TIPS method.

2.1 | TIPS technology

The first study, based on the preparation of a microporous polymer membrane, was conducted by Castro.[15] TIPS method presents more advantages in the fabrication of microporous polymer membranes than previously mentioned methods.[6,25] For example, with the TIPS method, the defects are easy to control, and there is a low propensity for its formation; TIPS is suitable for fabricating a diversity of quite thick isotropic microporous polymer structures for slow-release drugs.[26,27] Microporous polymeric materials have gained interest in various fields of applications, such as microfiltration, ultrafiltration, catalysis, medication delivery, clean energy, gas separation, and storage media owing to the particularly high porosity and surface area of these materials.[19]

Several polymers have been used to fabricate microporous structures using the TIPs method. They are: (i) polypropylene (PP)[6,28,29]; (ii) polyvinylidene fluoride (PVDF)[30,31]; (iii) poly(ethylene-co-vinyl alcohol) (EVOH)[32]; (iv) polystyrene[33,34]; and (v) polyethylene (PE).[6,25,29,35–37] The fabrication of microporous polyolefins has been widely investigated due to their cost and excellent thermal and solvent resistance. The fabrication of microporous polymer membranes using the TIPS method occurs through the following steps: (i) at high temperatures, the homogenous solution is formed by the combination of the polymer with the diluent or liquid (i.e., repellent). The liquid, in most cases, possesses a high boiling point and low molecular weight, making the polymer practically insoluble at room temperature[35]; (ii) After that, the mixture is rapidly cooled or quenched

to cause S–L or L–L phase separation; (iii) after the solvent extraction and drying the polymer strands initially containing liquid-repellent (typically by evaporation to guarantee the complete evaporation of solvent). The result is a microporous polymer membrane with the required structure.[6,25,38]

This work reports and describes in detail the information searched in the literature about the fabrication of microporous polymers as devices or reservoirs for insect repellent using the TIPS method. Figure 1 shows a representative phase diagram demonstrating the behavior of the phase of the polymer and repellent combination.[4] As can be seen in Figure 1, the metastable and unstable regions and the stable single-phase separation are exhibited by the system at an upper critical solution temperature (UCST). The phase diagram demonstrates how the matrix of microporous polymer is highly achieved when the amount of polymer is in a smaller phase than the repellent. The Flory–Huggins theory can be used to describe the loci of the phase boundaries in the polymer/repellent systems. This theory is described by the thermodynamic models presented below. At elevated temperatures above the UCST, the polymer/repellent system is fully miscible. Under this temperature, the phase separation takes place at a temperature that is influenced by the amount of the component of the system. In Figure 1, the two phases' compositions in equilibrium at any temperature. In the metastable region, the phase

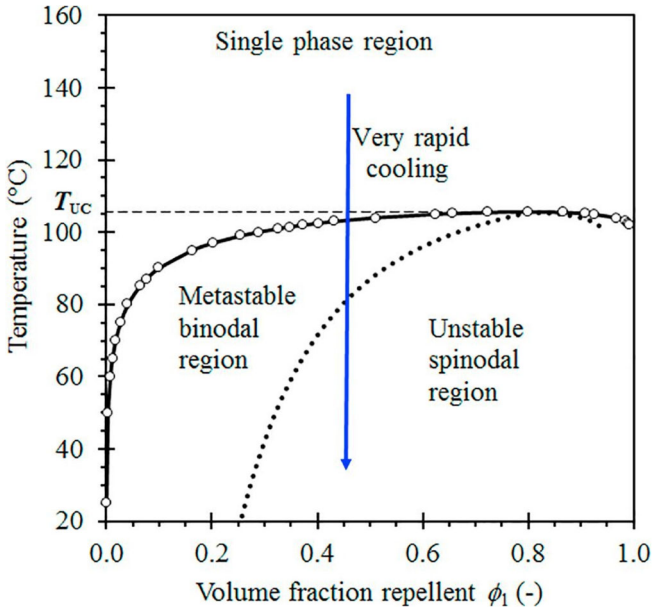

FIGURE 1 Fully-miscible polymer/repellent system demonstrated by the typical phase diagram. The binodal phase boundary is defined by a solid line and the spinodal envelope is represented by a broken line.[4] Reproduced with permission from Elsevier Science Ltd.

separation occurred through nucleation and growth mechanisms.[39] This is typical during L–L phase separation.[39] If the polymer represents the minor phase, it results in the unintended creation of distinct polymer particles that are deferred into a continuous repellent phase.

The spinodal curves are an additional set of phase envelopes that exist inside the two-phase area. This area of the phase diagram represents the thermodynamic full instability of a homogenous mixture. The solution divides into two phases on its own, as opposed to the metastable bimodal zone. Via a solvent-rich phase, a polymer-rich phase, and spinodal breakdown. This method of phase separation amplifies innate thermodynamic spatial composition changes through diffusion processes that result in a finely distributed microstructure. In the end, this cocontinuous structure might be stabilized by the polymer of the polymer/rich phase crystallizing afterwards. This implies that a substantial volume of liquid is trapped in a microporous polymer/rich phase structure. As previously described, such microporous polymer structures are frequently obtained through fast cooling of homogeneous polymer/repellent solutions melt in a bath of cold water.[4]

2.1.1 | Modeling porous polymer membrane obtained by TIPS technology

Thermodynamics and kinetics studies are fundamental in modeling membrane performance. The kinetics of phase formation, transfer rates, and thermodynamic potential differences control the intricate multiscale process of membrane development via TIPS.[40] It is challenging to observe and characterize the membrane formation process via TIPS using experimentation techniques alone due to the numerous variables, process speed, and complexity of the interactions.[8] As a result, modeling is an especially helpful technique for greatly advancing our comprehension of membrane formation. Modeling of membranes can be done using pore structure and pore size distribution. In the TIPS process, solvent molecules and polymer segments travel and interact at the molecular scale on length and time scales of nanometers (nm) and nanoseconds (ns), respectively.[10,41] The very thin interfaces that membranes create enable the selective transfer of heat and mass between various phases. Phase domains and various organized structures with typical length lengths of 10–100 nm form at the mesoscale during time scales of 10–1000 ns.[10] Macroscale analysis reveals that fluid dynamics, heat transfer, and mass transfer are three closely related transport phenomena that should be involved in membrane formation via TIPS. These three transport phenomena typically occur

simultaneously in physics and engineering science, and they can be described mathematically using similar techniques.[8] The fundamental physical and chemical laws, such as the laws of conservation of mass, energy, and momentum, serve as the foundation for these mathematical models. These laws are typically expressed by various types of continuity equations, which can be thought of as a more powerful, local form of conservation laws.[10]

Transport phenomena modeling in TIPS has been carried out since 1998 to forecast the shape and characteristics of the membranes as well as to characterize the heat transfer and compute the concentration profiles of various components.[42] In investigating the effects of various process parameters on the membrane structure, studies by Lloyd et al. focused on PP/diluent systems through a series of theoretical, modeling, and experimental studies. The casting film and bath were treated as finite and infinite domains, corresponding to the different parts of Figure 2. The variable l(t) denotes the (moving) position of the interface between them; continuity equations of the system are described in Equations (1) and (2).

$$\frac{\partial \rho}{\partial t} = \frac{\partial}{\partial z}(\rho v), \tag{1}$$

$$\frac{\partial \rho_2}{\partial t} + \frac{\partial}{\partial z}(\rho_2 v) = \frac{\partial}{\partial z}\left(\rho D_{23} \frac{\partial \omega_2}{\partial z}\right), \tag{2}$$

where, subscripts 2 and 3 refer to the diluent and polymer, respectively, D_{23} refers to the mutual diffusion coefficient of the diluent, ρ and ρ_i are the mass densities of the membrane solution and component i, respectively. ω_i denotes the weight fraction of component i, respectively, and v is the mass average velocity.

As shown in Figure 2A,B, The Krantz and Greenberg model (KG model) is used to model coupled heat and mass transfer. However, only heat transfer is considered when modeling the quenching process, whereas both mass and heat transfer must be considered during the evaporation stage.[8] This is because the polymer solution is made at a high temperature and is cooled below the spinodal decomposition temperature in the presence of an immiscible liquid to form the membrane after casting and a brief period of solvent evaporation that creates a gradient in the polymer concentration.[43] Mass transfer does not need to be considered at this point because the interactions between the cooling liquid and the polymer solution are negligible. Based on Fick's diffusion law of mass and heat, the evaporation model. However, in the case of the casting solution, Fourier's Law was used by the quenching model, as shown in Equation (3). The temperature profile evolution and component volume concentration were computed and found to be consistent with the membrane microstructure and thickness determined from the corresponding experimental observation.[15]

$$\frac{\partial T}{\partial t} = \alpha \frac{\partial^2 T}{\partial z^2}. \tag{3}$$

Furthermore, research studies by Barton and McHugh[44] on the prediction of the membrane pore morphologies, was the first TIPS modeling work, which computed the evolution of pore size gradients in the casting solution using a combination of simple heat transport and droplet growth rate kinetics. In the year 2016, Zhou et al.[43] developed a modified Maxwell–Stefan model that considers a cylindrical configuration to characterize the mass and heat transfer in the air gap and coagulation bath stages of the TIPS process.[43,44] The temperature and concentration fields of the system during the TIPS process were calculated to reveal the governing factor that determines the membrane asymmetry, and the model form was like Equations (1)–(3). In 2017, Manzanarez et al.[45] used water as a solvent instead of conventional organic solvents to develop a numerical model to investigate optimal operating conditions for the polyvinyl

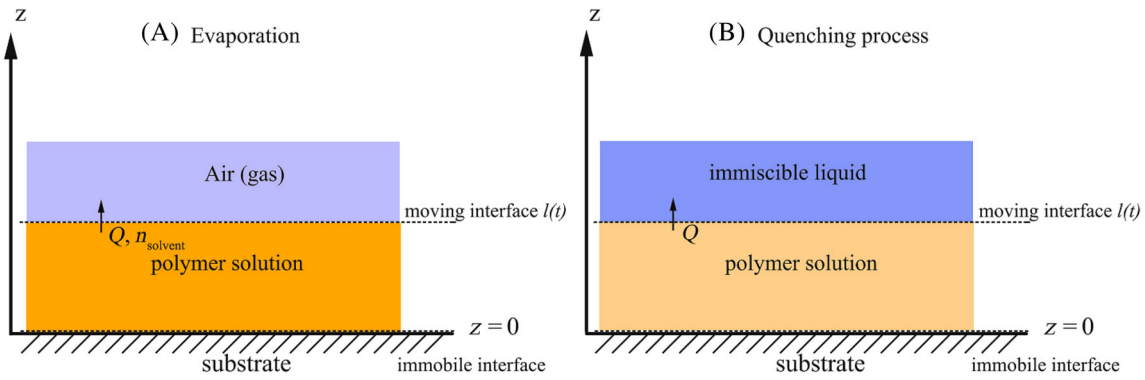

FIGURE 2 Schematic of the casting polymer solution and the surrounding "bath" for the TIPS processes. (A) and (B) represent the evaporation during the quenching period, respectively.[10] Reproduced with permission from Elsevier Science Ltd.

alcohol (PVA)/water system. The model was based on the Flory–Huggins theory, a specific diffusion formalism for dilute systems, and external mass transfer in free convection.[45,46]

During phase separation, the volume-averaged molecular concentrations are represented by continuous field variables that evolve in the phase field (PF) approach on time and length scales. PF approach is a powerful tool for modeling membrane formation processes on the mesoscale.[40] These field variables offer details about the local composition of a given phase at any given location and the locations of interfaces between distinct phase domains where concentration changes from one value to another.[10] The Cahn–Hilliard (CH) equation, which evolves conserved field variables, is a fundamental component of the partial fraction method. For multicomponent mixtures, the CH equation functions as a diffusion equation based on a presumptive thermodynamic model as shown in Equation (4).[8,10]

$$\frac{\partial \varphi}{\partial t} = \nabla . \left(M \nabla \left(\frac{\partial F_{\text{mix}}(\varphi)}{\partial \varphi} - 2K \nabla^2 \varphi \right) \right). \tag{4}$$

As represented in Equation (4), φ is a conserved field variable that usually denotes the local volume fraction of polymer in a polymer-solvent solution in polymer membrane formation research. The field variable's mobility is denoted by M, while the parameter κ scales the interfacial energy at the hetero-phase interfaces. The thermodynamic energy of mixing F_{mix} can be selected from a quantitative theoretical model, such as the Flory–Huggins model, where $F_{\text{mix}}(\varphi) = \Delta G_{\text{mix}}$. The description of the Flory–Huggins theory in polymer/repellent systems is described below.

In addition, some microscale molecular-scale simulation techniques, such as molecular dynamics (MD) and dissipative particle dynamics (DPD), have a particular advantage in simulating the membrane formation due to the trajectories of these individuals, and the molecular structure information can be directly involved.[47] This is because the molecular structure of the systems has a significant effect on the membrane formation, and the two methods (transfer and PF models) treat atoms and molecules implicitly. Representations of structures, such as membrane structure and pore size, are the results of molecular simulations that can be examined in relation to relevant phenomena.[48] The formation of a phase inversion membrane typically occurs over length scales of microns and time scales in the order of seconds, so it is obvious that an MD simulation cannot capture the entirety of the process. Consequently, because of its limitations on spatio-temporal scales, people tend to use the MD method to reveal the interaction between system components and calculate some important thermodynamic parameters, like solubility parameters, to support and validate the experimental results to optimize the membrane preparation parameters rather than using it to simulate phase separation.[10,48]

A summary of the modeling study revised in this work is displayed in Figure 3. The external field of the polymer solution was altered, which brought a sequence of changes, together with temperature and concentration alteration, phase separation, and phase inversion (polymer solidification), which controls the porous polymer membrane structure.

In conclusion, the membrane formation process can theoretically be replicated in computers due to the inherent differences in molecular simulation (of which DPD is a representative example) and the assumptions made regarding the forces or energetic interactions between segments of matter. Nevertheless, the molecular simulations' scales remain far from the real membrane because of the computational power limitation. According to the state of the most recent modeling research, it is anticipated that in the future, suitable multiscale modeling that covers the benefits of large-scale modeling techniques and has effective coarse-grained potentials derived from molecular tools will be developed to replicate the pore structures on specific systems of industrial interest.

In the field of polymer-based repellent delivery systems, Sungkapreecha et al.[49] and Akhtar and Focke[35] reported the polymer/repellent systems' phase behavior (i.e., LLDPE/Citronellal and PLA/DEET). The Flory–Huggins theory has been used to investigate the phase behavior of polymer/repellent systems. This theory is based on the methods that authors[50,51] proposed to characterize the thermodynamic aspects of polymer solutions. It's a lattice model where all solvent molecules and polymer segments are thought to occupy exactly one lattice site. Equation (5) of the Flory–Huggins model describes how variations in the size of the polymer and solvent or diluent molecules affect the mixing entropy.

$$\Delta G_{\text{mix}} = RT[n_1 \ln \phi_1 + n_2 \ln \phi_2 + n_1 \phi_2 \chi], \tag{5}$$

where ΔG_{mix} represents the mixing's molar Gibbs free energy; n_1 and n_2 represent the solvent and polymer moles that are present, respectively; ϕ_1 and ϕ_2 are the solvent and polymer volume fractions, respectively; the Flory–Huggins interaction parameter is represented by χ; R is the gas constant and absolute temperature is represented by T. Equation (5) can be rewritten as shown in Equation (6).

$$\Delta \overline{G}_{\text{mix}} = RT[(1-\phi_2)\ln(1-\phi_2) + (\phi_2/x)\ln \phi_2 + \chi(1-\phi_2)\phi_2], \tag{6}$$

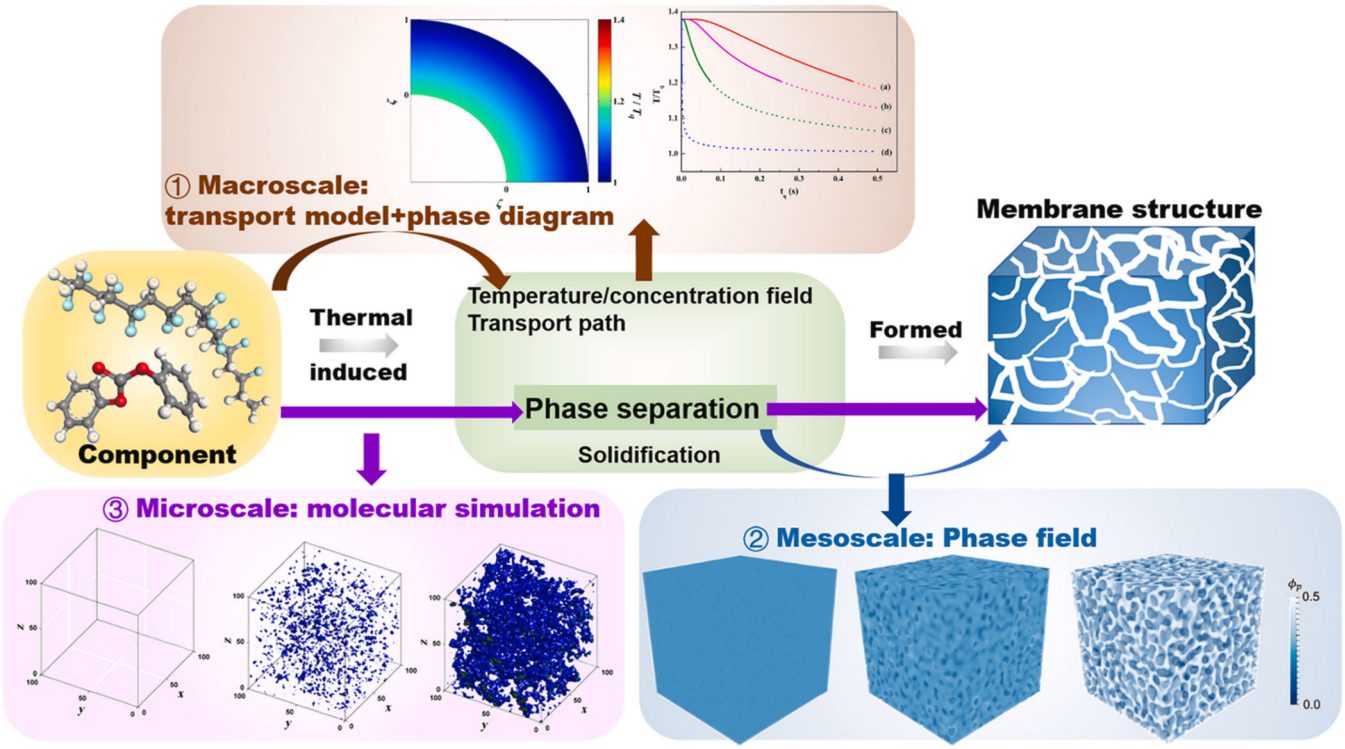

FIGURE 3 Modeling study summarized demonstrating the formation of porous polymer membrane via TIPS technology.[10] Reproduced with permission from Elsevier Science Ltd.

where the amount of mixing energy that Gibbs gives per mole of lattice sites is represented by $\Delta\overline{G}_{\text{mix}}$, and x represents the proportion of the solvent's molar volume to the polymer's (Equation 3):

$$x = (M_{n.2}/\rho_2)/(M_1/\rho_1). \tag{7}$$

To determine the Flory–Huggin's interaction parameter (χ) of the polymer/repellent systems as a function of temperature, Equations (8) and (9) proposed by McGuire et al.,[52] have been applied by Akhter et al.[33] and Matsuyama et al.[47] In TIPS processes, the diluent (liquid repellent) is a key factor in controlling the microporous polymer membrane structure. The thermodynamic properties have an immediate impact on the compatibility between the polymer and the diluent, including the temperature of crystallization and the binodal line.[8]

$$\left[\left(\phi_2^{\beta}\right)^2 - \left(\phi_2^{\alpha}\right)^2\right]\chi = \ln\left[\left(1-\phi_2^{\alpha}\right)/\left(1-\phi_2^{\beta}\right)\right] + (1-1/x)\left(\phi_2^{\alpha}-\phi_2^{\beta}\right), \tag{8}$$

$$x\left[\left(1-\phi_2^{\beta}\right)^2 - \left(1-\phi_2^{\alpha}\right)^2\right]\chi = \ln\left(\phi_2^{\alpha}/\phi_2^{\beta}\right) + (x-1)\left(\phi_2^{\alpha}-\phi_2^{\beta}\right), \tag{9}$$

where in the polymer-poor phase, the volume fraction of the polymer is represented by ϕ_2^{α}, and the polymer volume fraction in the polymer-rich phase is demonstrated by ϕ_2^{β}.

$$\chi = A + B/T. \tag{10}$$

An example of the Flory–Huggins interaction parameter for the systems LLDPE/Citronellal (Figure 4A) and PDLLA/DEET systems (Figure 4B) conforms with the linear behavior recommended by Equation (6) where UCST phase behavior is well explained by Flory–Huggins's theory with the interaction parameter χ exhibiting the following temperature dependence. The application of all equations above described the coexistence curves of binodal and spinodal coexistence are calculated and was previously shown in Figure 1.

3 | CRYSTALLIZATION STUDIES OF POLYMER IN SOLUTION WITH THE INSECT REPELLENT

As previously discussed, the phase separations between S–L and L–L display diverse kinetics studies to be used to identify the mechanism of separation. For example, for

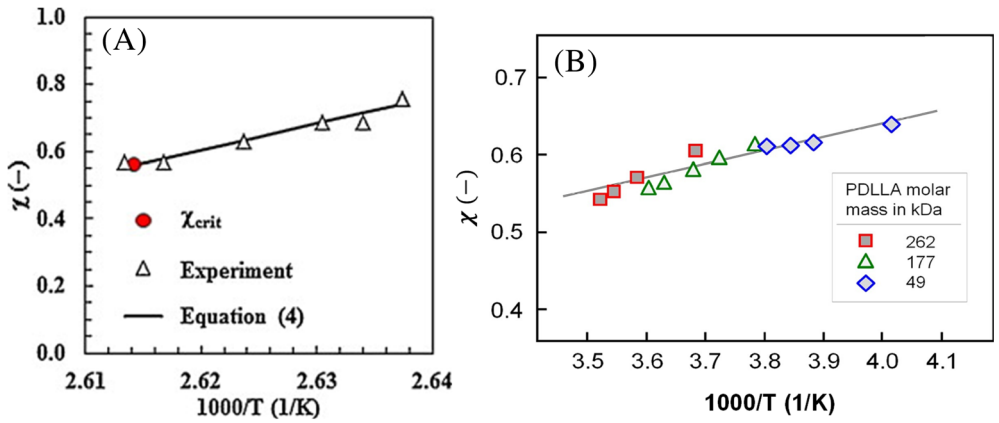

FIGURE 4 Flory–Huggins interaction parameter for the systems: (A) LLDPE/Citronellal[35]; and (B) PDLLA/DEET (different symbols represent data associated with PDLLA with mass-average molar masses of 49, 177, and 262 kDa).[49] Reproduced with permission from Elsevier Science Ltd.

spinodal decomposition, which occurs when the solution is thermodynamically unstable, the L–L phase separation is quick since the process is spontaneous.[9] L–L phase separation on the cooling of a solution under the spinodal phase transition line and remixing on heating takes place at similar temperatures.[9,13,53] On the other hand, crystallization in an S–L phase separation needs relatively high supercooling to produce crystal nuclei, and the crystallization and melting temperatures on the cooling and following heating are frequently not similar.[28]

There is often a dependence between the temperature of crystallization and the cooling rate due to the nucleation and growth mechanism.[9,54] The demixing behavior of polymeric materials solutions can be visually observed by cloud-point measurement. The measurements give details of the solution change in its optical appearance, commencing from clear toward turbid. The light scattering at phase boundaries is what creates the turbidity.[9,55] The limitation of the cloud-point measurement is that it does not give rapid details about the demixing mechanism (i.e., L–L and S–L phase separation). In general, the crystallization's kinetics, such as nucleation and growth mechanism, are discussed using Avrami Lauritzen and Hoffman's approaches.[56] The crystallinity's changes as a function of time and is estimated using the Avrami Equation, shown in Equation 11.[15] Therefore, this equation can be used to ascertain the degree of crystallization of the polymer-based repellent system.

$$X = 1 - \exp(-Kt^n), \tag{11}$$

$$\ln[-\ln(1-X_t)] = n\ln(t) + \ln(K), \tag{12}$$

where the polymer's volume fraction crystallized is represented by X at t, which represents time, a rate constant, which is dependent on temperature and relates to the rates of nucleation and crystal growth, is represented by K, and the parameter relating to the crystal geometry known by Avrami exponent is demonstrated by n.

The parameters of Avrami, such as n and K are obtained from the slope and intercept of an Avrami plot of $\ln[-\ln(1-X_t)]$ in contrast to $\ln(t)$. For isothermal crystallization, the K is determined by Equation (13).

$$K = \ln 2/t_{1/2}^n, \tag{13}$$

where $t_{1/2}$ is the half time. This is the time that is required for 50% of the total crystallization to take place.

On the other hand, the phase separation of polymeric solutions and the crystallization behavior of fully biodegradable or nonbiodegradable polymers have been studied by calorimetric and microscopic techniques.[57] DSC analysis has been employed to investigate the crystallization/S–L phase separation temperature of the polymer/liquid repellent systems and temperatures for phase separation (L–L) of polymer-based repellent systems. The polarized-light optical microscopy (POM) method has been used to investigate the crystallization behavior induced by S–L or L–L phase separation for systems of polymer-based repellents by visualizations of spherulite formation. The crystallization of polymers occurs in several steps; the process is preceded by crystal nucleation and primary and secondary crystallization.[58] The primary crystallization is characterized by quite quick space-filling spherulitic growth of crystals or lamellae. On the other hand, a secondary crystallization process is characterized by the existence of a slow perfection of crystals, with additional production of small crystals into the amorphous phases between the growths of crystals through primary crystallization, named by crystallization of insertion.[58,59] Various authors demonstrated that a biodegradable polymer known as polybutylene succinate (PBS) crystallizes abstemiously quickly under the equilibrium melting temperature ($T_{m,0}$) approximately at 130 °C.[60–63] The time interval of crystallization was approximately 1–10 s higher than the ambient temperature.[64,65] At supercooling, the melt-crystallization

proceeded by the growth of lamellae and the spherulite's formation.[58,66–68] The maximal crystal fraction is less than 50% because the molecular segments cannot diffuse into the intracrystalline chain-sliding.[58,69] Suppose crystal rearrangement is sped up by rapid heating; in that case, lamellae are formed at low melt-supercooling melt within a few degrees Kelvin above the crystallization temperature with a thickness below 10 nm.[69,70] Otherwise, crystal melting and lamellar thickening, then melt-recrystallization, occurs during slow heating.

Crystallization studies of biodegradable polymers, such as PBS and polylactic acid (PLA) at low melt-supercooling, have been well studied. This has been demonstrated by morphological information, such as pores size, crystal organization, and structure. Therefore, this information may be crucial since conventional melt-processing of biodegradable polymer (i.e., PBS) using extrusion, injection molding, or blow-molding usually consists of quick cooling or quenching using ice-bath water and solidification at low temperatures.[58,71–73]

In conclusion, by reducing the temperature until it is below the crystallization curve of equilibrium, all the products developed by TIPS can be frozen. The polymer crystallization rate and, in turn, the final polymer membrane structure are determined by the depth of the temperature reduction.[15] Upon crystallization of the phase rich in polymers when lamellae initially form and then grow in a spherulite structure. The diluent, or repellent, is moved from the growth front to the interlamellar areas—the spaces between the lamellae—as the lamellae form. Some droplets may be prohibited from the spherulites and form cavities between spherulites (interspherulitic areas), while others may be tricked between lamellae inside the spherulite (intraspherulitic or interlamellae areas), based on how quickly spherulites grow in relation to the diluent-rich droplet's mobility or diffusivity.[15,58,73] Impregnating by adding a suitable element or nanoparticles to a polymer-based diluent system is a typical technique for preparing Polymer blend TIPS membranes. A small number of nanoparticles added to polymer solutions act as nucleation sites, influencing the rate of crystallization and subsequent growth. These factors have a significant impact on the mechanical strength of the final polymer membrane, the porosity of the polymer, and the morphology of the crystals, particularly in S–L TIPS processes.[15] In general, Figure 5 shows four possibilities when the polymer-rich phase commences crystallizing: (a) two forthcoming spherulites interrupt and origin the deformation of a droplet (Figure 5A); (b) two droplets drive to each other at the growth of the spherulite (Figure 5B); (c) the movement of fluid origins a convective flow amid the spherulites (Figure 5C); and (d) droplet displacement produces huge micro voids (Figure 5D).[15]

Recently, studies on the crystallization behavior of polymers/repellent solutions prepared by TIPS technology have attracted more attention from researchers. For example, the crystallization studies of PBS in the presence of repellent DEET performed by DSC (Figure 6A,B) and POM (Figure 6C) were conducted by Yener et al.[64] Crystallization-controlled TIPS and the fabrication of a

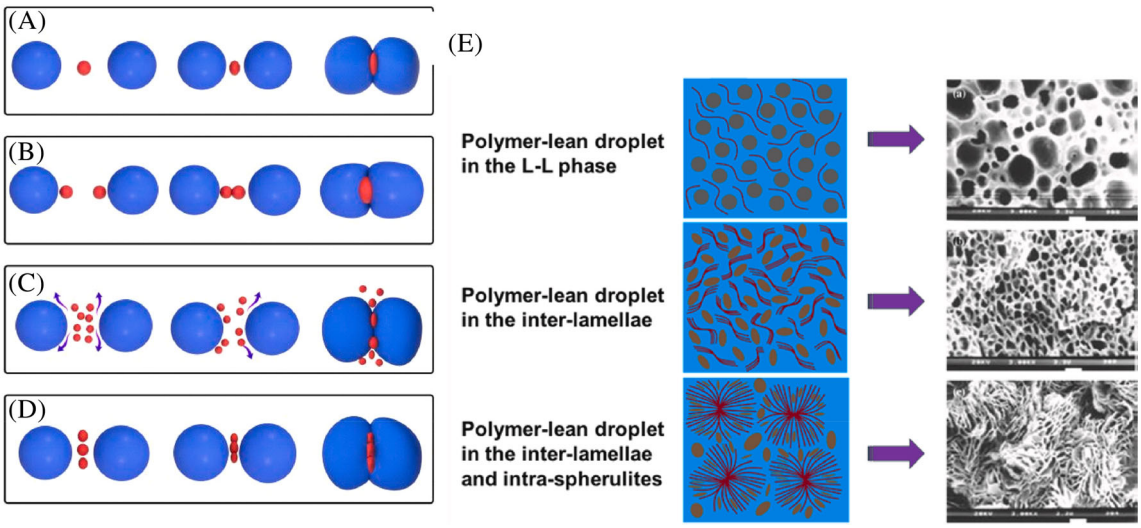

FIGURE 5 The schematic illustration demonstrates the deformation of a diluent-rich droplet during the effect of spherulitic boundaries (A); two drops coalescing amid two spherulites (B); a convective flow obtained between forthcoming spherulites (C); and the creation of huge macro voids in the connection amid spherulites (D). (E) Schematic description of polymer-lean droplets locking in the polymer membrane throughout polymer crystallization; and SEM images of polymer membranes.[15] Reproduced with permission from Elsevier Science Ltd.

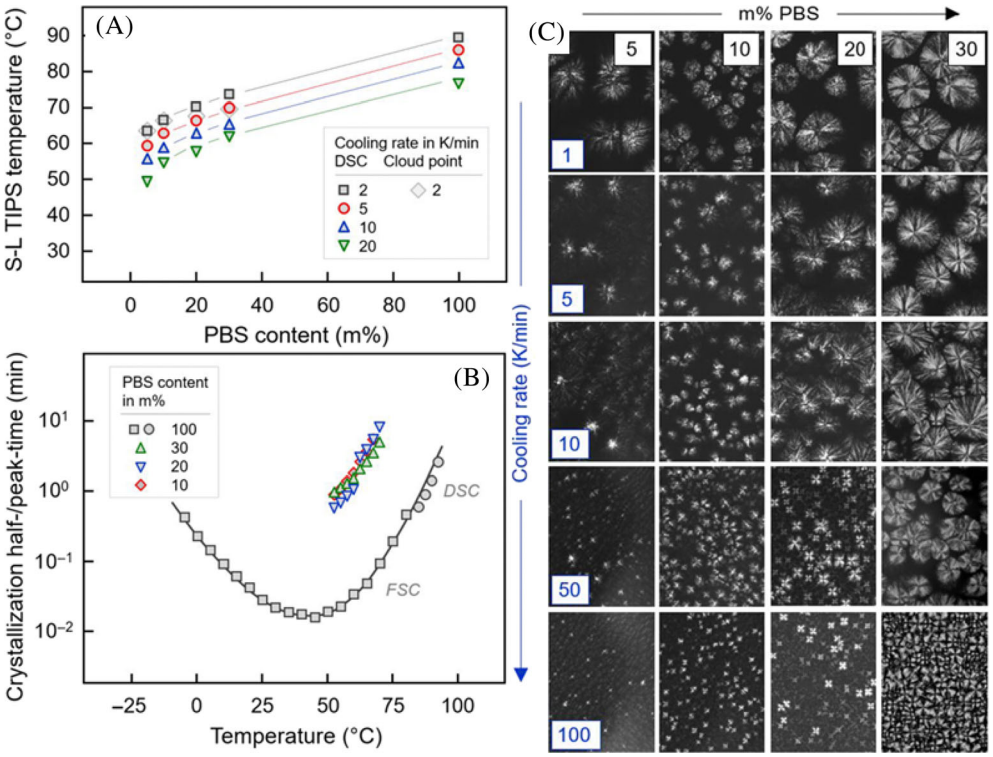

FIGURE 6 (A, B) showing DSC curves at transition temperatures in nonisothermal crystallization and (C) showing the POM morphology micrographs due to the rate of cooling.[64] Reproduced with permission from Springer.

spherulitic superstructure occurred when cooling the PBS/DEET solutions. The POM morphology was affected by the cooling conditions (Figure 6C). The influence of cooling rate on crystallization due to the general concepts, such as the interdependency of nucleation rate on temperature was affected; there was an enhancing quantity of nuclei/spherulites detected when the rate of cooling increased, this means whether crystallization/nucleation takes place at the elevated supercooling system. In addition, the concentration of polymers did affect spherulites/crystalline structures. For example, a higher quantity of spherulites/crystalline fraction was observed with increasing the amount of polymer.

In summary, the POM micrographs of PBS/DEET solutions led to the intermeshing of spherulites, aiming to produce mechanical stability instead of a rather liquid-like behavior, which was only detected for samples with 30 m% of PBS and, after quick cooling. Figure 6A,B shows the DSC quantitative results regarding transition temperatures in nonisothermal crystallization experiments as a function of the content of PBS. Several datasets, which were characterized with symbols/colors, demonstrated the influence of the rate of cooling and revealed the kinetics of the crystallization process. The reduction in the crystallization temperature was observed with enhanced concentration of repellent DEET. This was attributed to the equilibrium-melting temperature depression and the effect of dilution, slowing down both homogeneous nucleation and crystal's growth.[64,74–76]

Poly (L-lactic acid) (PLLA) is a polymer that dissolves into repellent DEET at high temperatures and crystallizes on cooling or quenching under concentration-dependent equilibrium melting temperature, producing scaffolds. Using DSC and POM techniques, the nonisothermal and isothermal crystallization behavior of PLLA/DEET solutions was investigated.[77] The nonisothermal (Figure 7A,B) and isothermal crystallization studies (Figure 7C) demonstrated that the crystallization behavior of the PLLA/DEET solution was quicker compared with the pure PLLA. However, the maximum rate of crystallization decreased with the reduction in PLLA concentration. The reduction in the crystallization rate as a function of the repellent DEET amount was attributed to the growth of the crystals reduction rate (Figure 7D) and the nuclei density. It was assumed that the presence of DEET contributed to the strong reduction of glass transition (T_g), and the increase in the mobility of chain segments of PLLA was considered the principal cause of the enhanced rate of crystallization compared with melt-crystallization of pure PLLA. However, the advantageous influence of enhanced mobility of chain segments is progressively compensated by the effect of dilution, which lengthens the needed diffusion path for the crystal's growth.

Figure 8A shows micrographs of different samples with 10–50 wt.% concentrations of PLLA. As can be seen in Figure 8A, spherulitic crystallization was observed, but regular variations were observed in the size of the spherulite and structure when changing the rate of cooling and

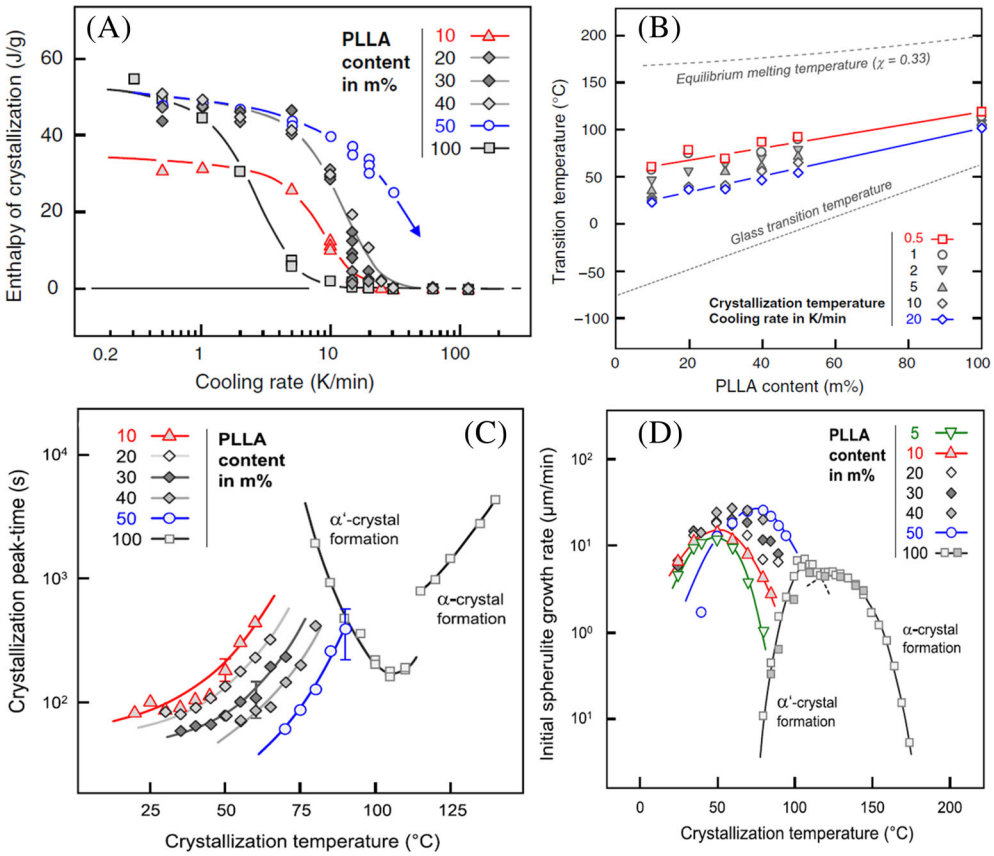

FIGURE 7 (A) and (B) show the nonisothermal and isothermal crystallization studies of PLLA, (C) and (D) show the crystallization behavior of PLLA/DEET solution.[77] Reproduced with permission from Wiley.

concentration or composition of PLLA and DEET. In addition, the POM method was explored to investigate the morphology of the PLLA/DEET system after isothermal crystallization at three different temperatures (60, 70, and 80 °C) (Figure 8B). The POM micrographs of the samples revealed important information, such as: (i) For certain compositions, the nuclei density increased with a reduction in the temperature of crystallization; (ii) The nuclei density decreased with a reduction in the amount or concentration of PLLA at a certain temperature of crystallization. As a result, at room temperature, the remaining liquid solution after crystallization may form a distinct continuous interspherulitic phase or be confined between spherulites.[77]

4 | MORPHOLOGICAL STUDIES OF POLYMER DEVICES OF INSECT REPELLENTS

The microporous polymer membranes applied in the drug delivery field in tissue engineering, the ideal scaffold should be three-dimensional (3D), extremely porous, and have a permeable structure containing a homogenously distributed and interconnected open-cell porous network.[78–80] Furthermore, suitable pores (size, shape, and wall morphology) are required. Overall, morphological properties (pore size and porous structure) of polymer membranes are highly dependent on the quenching or cooling conditions. Quick cooling provides a range of nuclei and reduces the amount of time needed for crystal growth, while slow cooling offers extended times for crystal growth, ensuing in polymer membranes fabricated by L–L separation with crystallization step following. Generally, a porous, cellular-like, and/or continuous structure is most often formed.[81] On the contrary, the microporous polymer membranes obtained through S–L phase separation have demonstrated spherulitic structures.[81] Recently, Focke's research group has developed an approach to fabricate microporous polymeric materials-based insect repellents by melt blending using TIPS technology. Several problems related to the low interconnectivity, low void volume, inadequate control over the size and distribution of pores, and challenges in obtaining materials with consistent porosity of the polymeric materials have been resolved by the research group.

4.1 | Morphological study of polyolefin devices of insect repellents

Polyolefin is a low-cost polymer considered to be physically, chemically, and thermally stable, with good

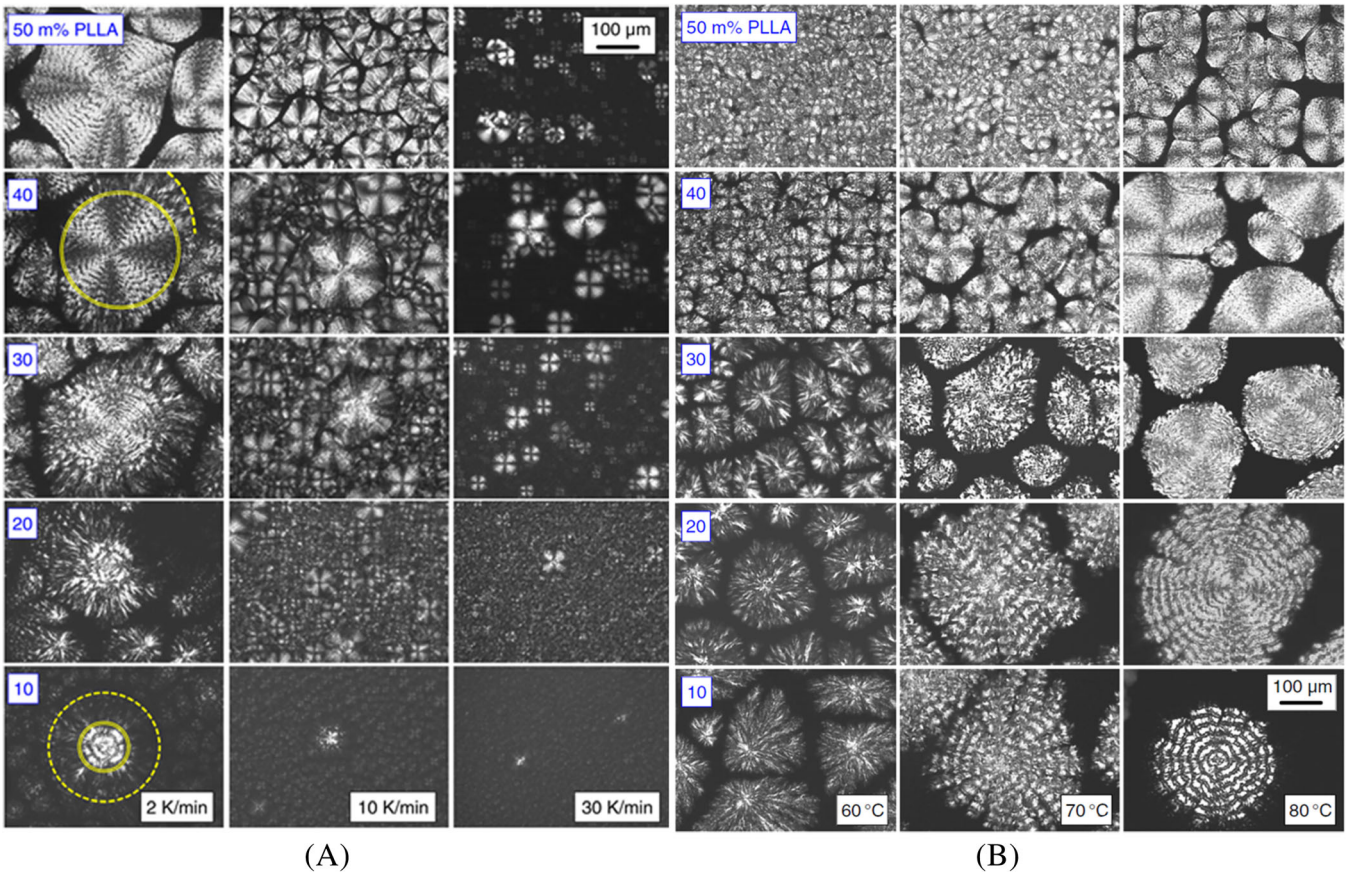

FIGURE 8 POM micrographs show (A) PLLA/DEET systems with various concentrations (10–50 wt.% PLLA) obtained after cooling at rates of 2, 10, and 30 K/min; (B) PLLA/DEET systems containing different concentrations of PLA (10–50 wt.%) produced after isothermal crystallization at 60, 70, and 80 °C.[77] Reproduced with permission from Wiley.

mechanical properties. Nowadays, polyolefin is widely used to produce membrane materials for several applications.[82] However, with contact angles between 100 and 120 °C, their membranes have low hydrophilicity, necessitating improvement of their surface wettability.[15] Conventional diluents have poor eco-toxicological profiles because of the nature of the polymers that are extensively used for the TIPS process. Several research works have demonstrated a success in fabrication of microporous membranes using main diluents such as mineral oil (MO),[6,83] diphenyl ether (DPE),[84–86] liquid paraffin (LP),[27,36,87–91] decalin,[86,91] diisodecyl phthalate (DIDP),[36,92] dodecanol/soybean oil (SBO),[86] isoparaffin,[63] soybean oil (SBO),[68] dioctyl phthalate (DOP), dioctyl phthalate (DOP)/polytetramethylene glycol (PTMG), soybean oil (SBO)/poly(tetramethylene glycol) (PTMG).[93] The common polyolefins used in the fabrication of microporous polymer membranes include LDPE, HDPE, UHMWPE, EVA, and PP.[82]

Scanning electron microscopy (SEM) is the most important method of analysis used to investigate the morphology in the polymer field. Therefore, in the case of polymer-based repellent devices, the morphological studies can give enough information on how the microporous structure known as reservoirs trapped large amounts of the liquid repellent and how the concentration of polymer, repellent, and type of polymer, repellent, and fillers as well as cooling rate which can influence on the morphology of the polymer membrane devices.

The first study regarding the fabrication of microporous polyolefin membranes as devices for insect repellent citronellal using the TIPS method was done by Akhtar and Focke.[35] The system of LLDPE/Citronellal was obtained by a simple melt method where the samples were placed in an oven at 150 °C to permit its homogenization state. After that, the LLDPE matrices containing citronellal were quickly submerged in ethanol and ethylene glycol mixtures containing crushed dry ice to quench-cool them. Different quenching solvents, such as ethanol ethylene glycol, were chosen to obtain quenching temperatures of −18, −14, and 5 °C.[94] Liquid nitrogen was used to quench another sample (ca. −170 °C). It is important to note that this study demonstrated that an effective way to change the heat rate and mass transfer

during the quenching period of a TIPS method is by adding a solvent to the quenching bath. These solvents have the property of increasing the bath's viscosity, resistance to heat transfer, and rate of solvent–nonsolvent exchange. For microporous polymer membranes prepared via TIPS technology, the porous structure happens throughout the formation of the polymer membrane. The solvent difference between the polymer/diluent solutions and the quenching bath can be minimized by adding solvent to the latter and may consequently affect the TIPS process, altering the relatively large quantity of the equivalent structures in the final membrane.[15] Quenching homogeneous melt mixtures results in a microporous structure with submicronic pores (Figure 9). Because the liquid citronellal was trapped inside the polymer framework and held there by capillary forces, it was effectively solidified. The impact of quenching temperature on LLDPE/Citronellal system morphology (40 wt.%/60 wt.%) was confirmed using SEM analysis (Figure 9). The temperature of quenching used varied from 5 °C to that of liquid nitrogen. There is a correlation between the cooling rate and the quenching bath temperature. In the TIPS technology, this causes phase separation and regulates the development of the microporous polymer membrane. According to recent research based on the TIPS process, the temperature at which the polymer is quenched affects mass and heat transfer, which controls the membrane structure, including bi-continuous and macro void structures in various regions.[15,23,95]

Furthermore, by modifying the bath's composition (such as adding an organic solvent), the mass transfer in the TIPS method can be precisely controlled. Furthermore, considering the need for environmentally friendly industrial processes and the restricted environment strategy, the use of green and eco-friendly additives has been highly recommended. Considering sustainability and the promotion of green chemistry principles, this research path merits more attention.[15] According to SEM micrographs, it was possible to observe that over that temperature range, all samples presented a different morphology. The cocontinuous structure seen by SEM suggested that spinodal decomposition was, in fact, the cause of the phase separation (Figure 9A–D). For all the samples investigated, the typical pore sizes were less than 1 μm. Therefore, as capillary forces increase with decreasing pore diameter, it is likely that they effectively retain the liquid repellent in the fine open-cell polymer foam.

Additionally, hot-stage optical microscopy is used to determine the cloud point and the behavior of crystallization of the LLDPE/Citronellal system (Figure 9E–G). The LLDPE/Citronellal formulations were heated above the melting temperature of LLDPE to obtain full miscibility between LLDPE and Citronellal; afterwards, these

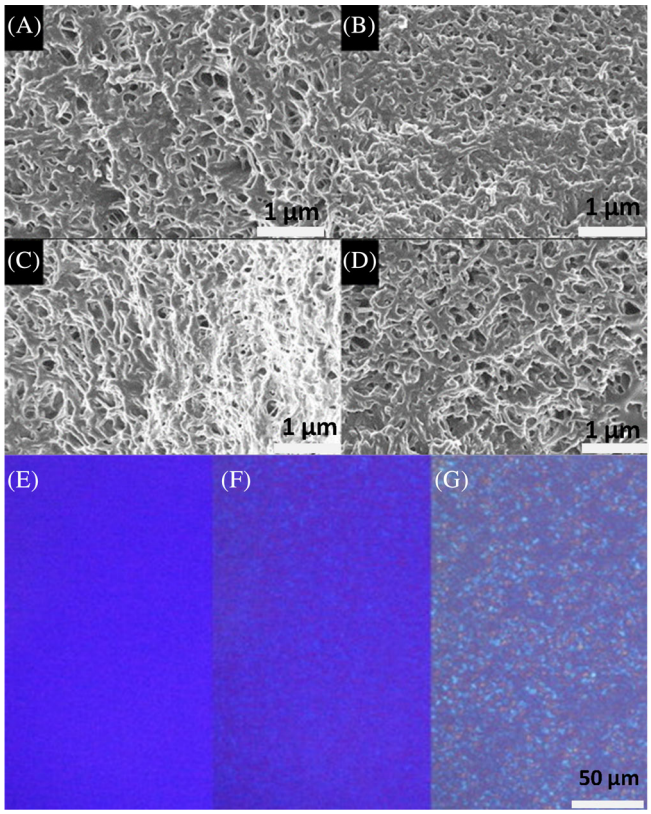

FIGURE 9 SEM micrographs of LLDPE/citronellal (40 wt.%/60 wt.%) were prepared using the TIPS method. Different morphology of the polymer-based repellent was obtained by different quenching temperatures: (A) −171 °C (liquid nitrogen); (B) −18 °C; (C) −14 °C, and (D) 5 °C. Optical micrographs of the phase changes LLDPE/Citronellal (70 wt.%) showing (E) a Homogeneous mixture at 140 °C; (F) the appearance of turbidity at 108 °C, and (G) the solidified crystalline material at 80 °C.[15] Reproduced with permission from Elsevier Science Ltd.

were cooled at a constant rate (10 °C/min). The micrographs showed that various spots were observed at the cloud point. Furthermore, after cooling, the crystallization in the LLDPE/Citronellal mixtures took place.

From the work done by Akhtar and Focke,[35] new advances in the development of microporous polyolefin strands as slow-release devices for repellent via the TIPS method using synthetic repellents (DEET and Icaridin) as a diluent were conducted by Mapossa et al.[4] The extrusion compounding was used to fabricate linear low-density polyethylene (LLDPE) devices for repellents. The extruded strands were quickly cooled in an ice water bath to allow the microporous polymer fabrication. The effect of the repellents DEET and Icaridin on LLDPE strands was investigated by SEM analysis. Additionally, additives (fillers) such as Dellite 43B organo-modified clay and pyrogenic silica were added into LLDPE polymer, and their impact on the polymer matrix was investigated using SEM

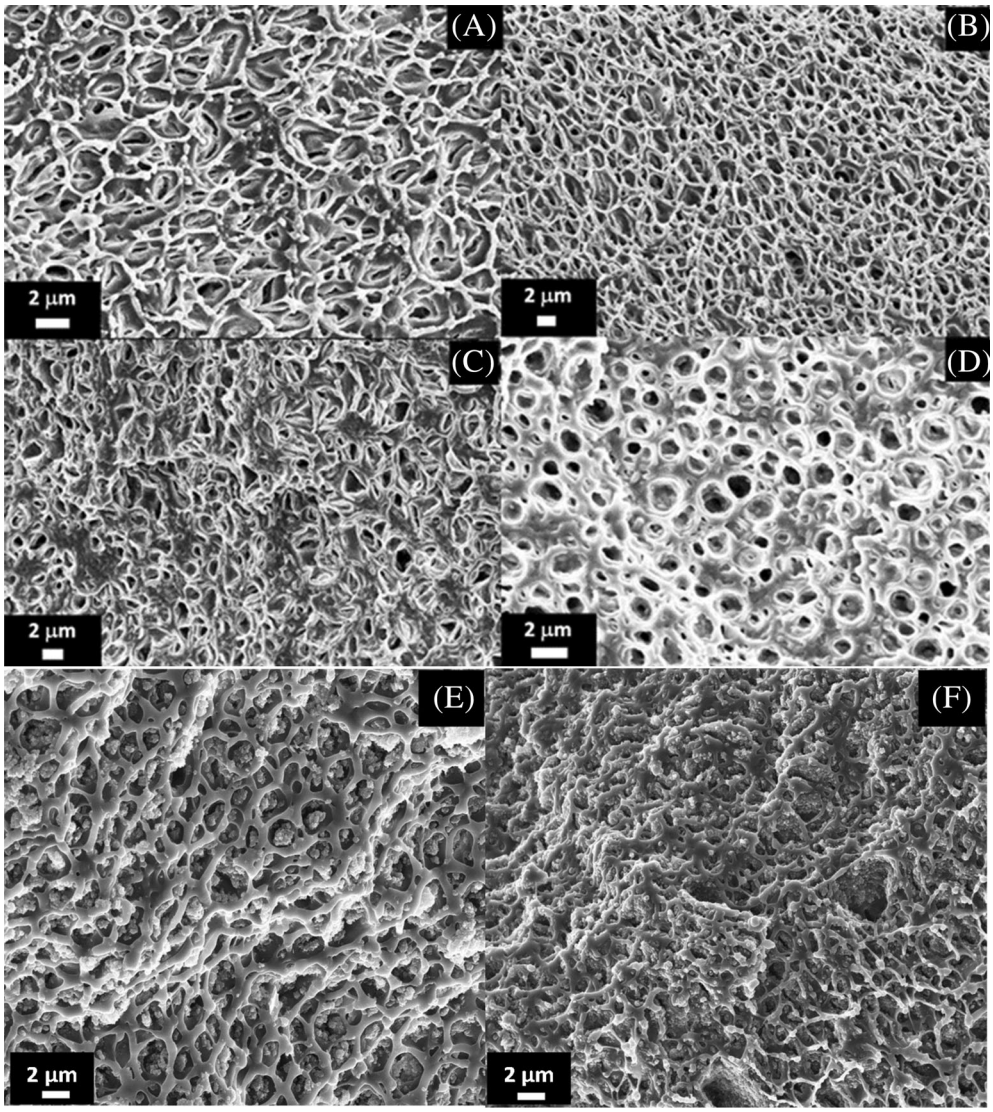

FIGURE 10 SEM micrographs demonstrating the effect of type of insect repellent and its concentration on the morphology of LLDPE strands containing: (A) 20 wt.% DEET; (B) 30 wt.% DEET; (C) 20 wt.% Icaridin; (D) 30 wt.% Icaridin. A 5 wt.% of clay was added to all LLDPE strands. Influence of silica and type of repellent on the morphological structure of LLDPE strands contained: (E) 30 wt.% Icaridin; (F) 30 wt.% DEET. A 5 wt.% of silica was added to all LLDPE strands.[4] Reproduced with permission from Elsevier Science Ltd.

analysis. The effect of the repellents' nature and their concentration on the phase morphology of LLDPE, evidenced by the solvent extraction method, was presented in Figure 10. The SEM micrographs showed that the nature of the microporous LLDPE strands observed was uniform with the anticipated cocontinuous structure when spinodal decomposition caused the phase separation.

Nevertheless, it was evident from the SEM micrographs presented in Figure 10 that the type of insect repellent and its concentrations incorporated into LLDPE strands greatly affected the final microcellular LLDPE structure. According to the authors, these had difficulties in describing the spatial organization of these open-cell foams. The LLDPE-based-DEET samples presented a scaffold highlighting a filamentous structure (Figure 10A,B). For samples based on the LLDPE/Icaridin system, its microstructure is demonstrated to have a more cellular appearance containing close spherical cavities unified through smaller avoids (Figure 10C,D). In summary, for all samples, the scale of cavities or holes was in the order of a few micrometers.

A remarkable observation was that, in all samples, there were no clay platelets observed on microporous LLDPE devices, which suggested that the filler platelets had been restricted to the microporous scaffold structures' polymer-rich phase (Figure 10E,F) showed the effect of fumed silica and the nature of repellent on the morphology of the extruded LLDPE matrix. The SEM micrographs of the LLDPE matrix changed when the fumed silica was added, thus affecting the structure of the microporous polymer strand. Additionally, the micrographs indicated the presence of fumed silica particles that were aggregating inside. This suggested that the fumed silica mainly existed in the repellent-rich phase after phase separation was complete. This behavior was most visible for the strands based on LLDPE with Icaridin (Figure 10A,B), where the pore sizes are bigger than those of LLDPE with DEET systems (Figure 10C,D).[4]

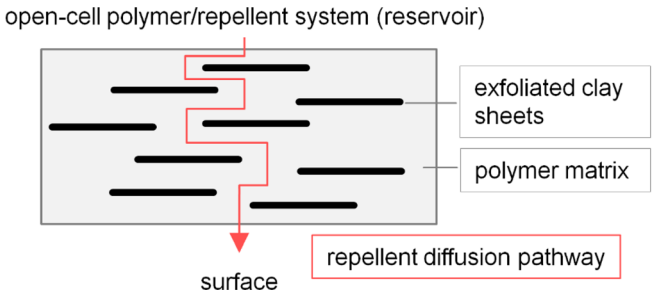

FIGURE 11 Illustration of the exfoliation of the clay platelets into the polymer matrix to control the effective repellent diffusion path.[96] Reproduced with permission from Springer.

In summary, it is important to understand that additives/fillers interactions meaningfully influence the solution demixing phenomena, hence influencing the microporous polymer membrane morphology and its activity.[23] For example, additives influence the binodal line location, which brings a thermodynamic effect by either initiating or delaying the crystallization behavior of the polymer (kinetic effect). The polymer membranes can be affected by additives in ways such as: (i) They can form pores that improve the membrane permeability; (ii) They can alter the surface properties, changing the hydrophilicity or hydrophobicity of the membranes; (iii) Lastly, additives can improve the membrane mechanical properties.[23] The filler of 5 wt.% Dellite 43B clay was added in all samples to obtain the full exfoliation of the nanoparticles into the polymer matrix to control the volatility of the repellents from the membrane polymer structures to the outer surface of the microporous polymer-based repellent known as a reservoir for a large quantity of active ingredient (Figure 11).[96] The addition of clay (<10%) in the polymer matrix results in the improvement of the mechanical, thermal stability, and permeability properties and improves the compatibility of the active ingredients into the polymer.[16,97] These improvements are beneficial in the pharmaceutical industry.

As the idea of the research work by Mapossa et al.[96] was to develop LLDPE as devices to control the release rate of insect repellent to be used to control malaria transmitted by mosquitoes in endemic regions, the SEM analysis was used to investigate the existence of membrane and the thickness of the membrane that covers the polymer-based repellents strands. SEM micrographs in Figure 12 showed the morphology (outer surface) of an LLDPE strand primarily containing DEET. The noticeable border observed in the cross-section view (Figure 12A**)**, the side-view (Figure 12B), the smooth outer surface (Figure 12C,D) and the presence of a skin-like membrane that covered the microporous LLDPE strands were

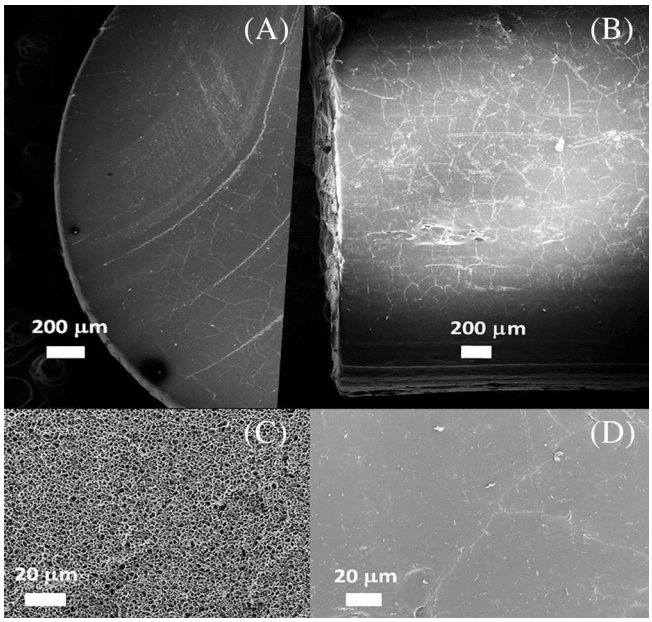

FIGURE 12 SEM micrographs showing: (A) a Cross-section of the extruded LLDPE strand; (B) a side-view of the cut strand; (C) the appearance of the microporous inner surface contrasted with (D) the outer surface appearance of the polymer skin.[4] Reproduced with permission from Elsevier Science Ltd.

observed by SEM. The observation suggested that the high quantities of repellents, such as DEET and Icaridin can be well trapped in the microporous LLDPE, and it can be controlled by its release by the membrane of LLDPE. This is an advantageous aspect since the work was designed to fabricate microporous polymer membranes capable of guaranteeing effective protection of people against mosquito bites for an extended period.

According to research by Akthar and Focke[35] and Mapossa et al.,[4] temperature has a significant impact on the morphology of product-based polymer/repellent systems. Raising the temperature of the polymer/repellent system causes its viscosity to decrease and the temperature of the gradient to rise via the TIPS process, which influences phase separation and promotes heat transfer. Yet, because most repellents have boiling points above 200 °C and above the cloud point, the drug (repellent) TIPS processes typically have temperature restrictions. Rather, it ought to be between 25 and 200 °C below the boiling point of the repellents (diluents).[15] To achieve high performance of LLDPE membranes in systems without a cloud point, the profile of extrusion temperature should be higher than the polymer-based repellent solution's crystallization temperature.[4]

By adjusting the solution's temperature, the structure and activity of the microporous polymer membrane can be modified. Therefore, in the TIPS technique, high diluent evaporation at the air gap during the membrane

preparation process due to an elevated temperature (typically >200 °C) enables an increasing polymer surface concentration. This induces the formation of a dense layer on the membrane surface, which significantly reduces the membrane permeability. Furthermore, the diluent evaporation similarly affects the membrane sub-layer, resulting in the formation of a dense structure.[15,98] Although there are some traditional methods capable of addressing this issue, such as decreasing the air gap distance, increasing the temperature at the air gap, and increasing the extrusion rate, the membrane surface and sub-layer morphological structures (e.g., bi-continuous network density, spherulitic size, and lamellae thickness) are difficultly engineered to achieve some specific application requirements.[98] A denser outer surface of the microporous LLDPE strands with reduced membrane permeability was produced by Mapossa et al.[4] (Figure 12). Additionally, the LLDPE-based repellent systems prepared by extrusion demonstrated greater consistency of the porous where the cocontinuous porous was formed.

Due to some advantages of EVA compared with LLDPE, such as its special molecular structure and modifiable characteristics associated with vinyl acetate content,[99,100] EVA produces soft material membranes that can be applied as potential devices of repellent due to the materials being more comfortable for wearing. Because EVA is a commercially available, biocompatible, and nontoxic polymer, it is also frequently applied as a biomaterial[101] for medical applications.[80] Additionally, because of its stability, EVA is a popular scaffold material for drug delivery (i.e., repellents) over an extended period. With the consideration of the advantages associated with EVA, Sitoe et al.[95] demonstrated, via TIPS, the possibility of fabricating microporous EVA with DEET using extrusion compounding. The produced EVA strands-based repellents were to be applied in malaria control. The visualization of microporous EVA strands was done using SEM analysis, and it was an important task as open cells could act as reservoirs for large quantities of repellents. Thus, SEM micrographs of EVA primarily contain 20 and 40 wt.% of DEET and 30 wt.% of Icaridin are shown in Figure 13A–C. The nature of the repellent and the type of fillers (clay or silica) also did affect the morphology of the EVA matrix.

The extruded strands had a translucent appearance; this was the case before the extraction of repellent from the EVA matrix using solvent dichloromethane. However, after the extraction of DEET from the EVA matrix by solvent and drying the EVA matrix, the strands appeared to be dense white for EVA-based DEET with clay. This suggested there was the uniformity of open cells with the interconnection of porous structures into the EVA matrix. This was confirmed by SEM analysis (Figure 13A). Furthermore, the clay platelets were also clearly visible in the EVA matrix (Figure 13A). The SEM micrographs of EVA strands initially containing 40 wt.% DEET and added pyrogenic silica as the nanofiller is shown in Figure 13B. The agglomeration state of silica into the EVA matrix was well visible along the EVA structure where the open cells were not uniform, demonstrating that the filler was related to the DEET-rich phase.

In the case of EVA samples initially containing Icaridin, a dense with no uniform porous structure was observed (Figure 13C). This was caused by a high degree of shrinkage of the EVA scaffold observed after leaching the Icaridin by solvent.[4]

Recently, a study on the preparation of LLDPE and EVA impregnated with plant-based repellents (essential oils, that is, carvone and spearmint essential oil) was conducted by Phala et al.[16] The aim of the investigation was to use LLDPE as a device to trap essential oils for antibacterial applications. The authors followed the methodology used by Mapossa et al.[4] to prepare LLDPE strands. The effect of the repellent type, concentration, and type of polymer on the morphology of the prepared polymer matrices was evaluated by SEM analysis, as shown in Figure 14. As demonstrated in Figure 14A–I, high quantities of porous structure with different pore sizes were observed on the surface morphology of all extruded polymer strands. These pores serve as evidence that spinodal decomposition phase separation can produce a homogenous polymer and active ingredient-rich mixture. Additionally, it is likely that the outer layer of dense skin acts as a diffusion barrier to regulate the release of the active ingredient at sufficient levels over prolonged periods of time. The differences between the microporous nature of the two polymer strands and the type of repellents used were observed. The SEM micrographs demonstrated that a more interlaced structure with well-defined pore sizes was produced for the extruded LLDPE strands.

On the other hand, interlaced cavities with various sizes arbitrarily distributed into the extruded EVA matrices were observed. In summary, the type of polymer and repellent did influence the final morphology (i.e., microporous structure) of the polymer. In addition, also it was found that the concentration of repellent contributed to the difference in microporous structures of polymer matrices. In all extruded LLDPE and EVA-based repellent strands, the clay was added.

4.2 | Morphological study of biodegradable polymer devices of insect repellents

Although the studies mentioned by researchers above have demonstrated success in the fabrication of

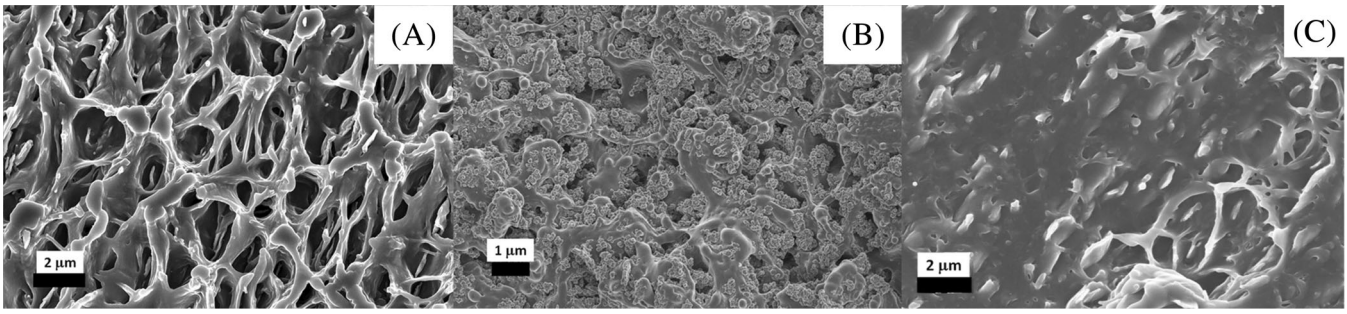

FIGURE 13 SEM micrographs showing the internal structure region of extruded EVA strands. (A) 20 wt.% DEET with 5 wt.% of clay; (B) 40 wt.% of DEET with 5 wt.% silica; (C) 30 wt.% of Icaridin containing 5 wt.% of Dellite 43B clay.[95] Reproduced with permission from Wiley.

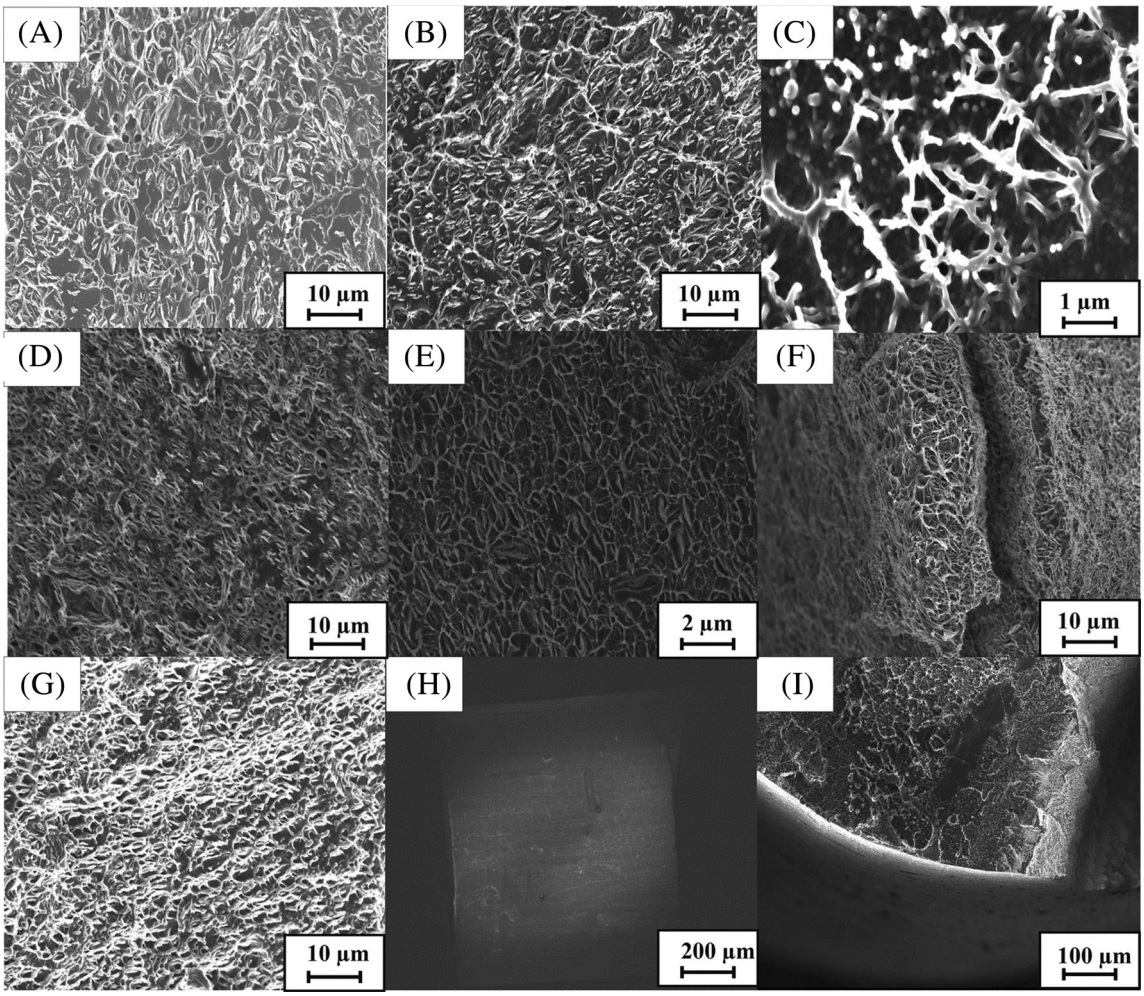

FIGURE 14 SEM micrographs showing the carvone or spearmint effects on the structure of the internal microporous region of extruded EVA and LLDPE strands. (A) EVA/carvone (20 wt.%), (B) EVA/spearmint (20 wt.%), (C) EVA/carvone (30 wt.%), (D) LLDPE/carvone (20 wt.%), (E) LLDPE/spearmint (20 wt.%), (F) LLDPE/carvone (30 wt.%), (G) LLDPE/spearmint (30 wt.%), (H) outer surface of extruded EVA strand appearance and (I) membrane covering extruded LLDPE filaments.[16] Reproduced with permission from Elsevier Science Ltd.

microporous polyolefin as devices for insect repellents via the TIPS method, these are nonbiodegradable polymer-based-petroleum. Therefore, the concern related to the mismanagement of waste in the world is already affecting human and environmental health. Scientists have maximized their efforts in using biodegradable polymers in

their research as potential alternatives to replace nonbiodegradable polymers in several fields (i.e., drug delivery).[9,64,96,102] Nowadays, PLA has attracted a lot of interest from researchers in the preparation of scaffolds[103–105] and foams[106] because of its peculiar property profile. Cellulose acetate (CA) is another noteworthy bio-based polymer. It is commonly utilized as cellulose triacetate (CTA) and has potential uses in medicine because of its high hydrophilicity, plenty of precursors, and biodegradability.[102]

PLA is an aliphatic polyester that is environmentally friendly and obtained from short-term renewable resources. PLA can be applied in different fields due to its compost ability, food safety compliance/FDA approval, and biocompatibility.[107–109] PLA is produced from lactic acid from two optically active forms, such as L- and D-lactides, allowing the production of PLLA homopolymer and random (D, L-lactide) copolymers (PDLLA).[9] On the other hand, PLLA is considered an active form of PLA that is capable of partially crystallizing. The existence of D-isomer counits in L-isomer-rich chains deteriorates crystallization and leads to a decrease in the maximum reachable crystallinity; PLA with more than 10% D-isomer counits is amorphous or displays only insignificant crystallinity.[58,110] As crystallinity controls bio-resorbability, special, noncrystallizable random PDLLA grades have been employed in the biomedical field.[9]

Previous studies have demonstrated that porous PLA can be formed by the TIPS method using organic solvents, such as dioxane/water,[103] chloroform/methanol,[14] tetrahydrofuran (THF),[106] or dichloromethane/hexane.[111] Concerning efforts to create phase diagrams for solvent-rich systems of the PLA/dioxane/water system, it was confirmed that a liquid–liquid (L–L) phase separation takes place at a high ambient temperature through the demixing temperature, enhancing the concentration of the polymer.[14] For crystallizable PLLA, the L–L phase separation leads to the crystallization temperature throughout cooling or quenching. Additionally, in the PLA/chloroform/methanol systems, it was suggested that, because of the elevated activation energy required for crystallization, the L–L demixing frequently leads to solid–liquid (S–L) demixing; nevertheless, the order can be changed by the selection of the optimum conditions, such as cooling or the concentration of the polymer.[14]

Until the year 2016, there was no study explored regarding the miscibility and demixing of the biodegradable polymer (i.e., PLA/DEET) system as a carrier for repellent in the biomedical field. Therefore, the first study regarding the fabrication of microporous biodegradable polymer membranes as devices for insect repellents using the TIPS method was conducted by Sungkapreecha et al.[9] The phase diagram of the PLA/DEET binary systems, where the aim was to investigate the potential application of biocompatible and biodegradable PLA as a reservoir device for large amounts of insect repellent known as DEET was established by Sungkapreecha et al.[9] The production of PLLA spherulites and solid structure on slow quenching/cooling of the PLLA/DEET system from 150 °C to ambient temperature is shown in Figure 15. The SEM micrographs demonstrated in Figure 15A–C are large spherulites corresponding to 50–100 mm. Similar sizes were confirmed with the POM micrograph, as shown in Figure 16. The SEM micrographs show the PLA crystals in which spherulites are growing with slow quenching or cooling of the solution of the PLLA/DEET system. Therefore, an intraspherulitic scaffold-like structure (i.e., pore size less than 10 mm) was formed, but the scaffold structure was lost at the spherulite boundaries. It is important to note that the PLLA/DEET system was prepared on a very small scale, where the polymer/repellent mixture was placed into the glass vial and closed. The dissolution was executed at 150 °C by a Thermo Scientific Reacti-Therm block heater/stirrer.

The creation of spherulites, for instance, which grew from point-like nuclei, is clearly seen in the POM micrographs, as seen in Figure 16.[9] The samples show multiple of these spherulites within the field of view, but they are all separated from one another at their edges. This separation is probably caused by the solution's lack of crystallizable polymer, particularly in the sample with just 5 wt.% PLLA (Figure 16A), the low concentration of polymer in the solution only permits dendritic-like crystal formation, even near the nucleation spot. Dendritic growth is less likely to occur at greater PLLA concentrations; however, it is still noticeable in the spherulites' outer portions. However, no qualitative variations in the spherulite structures were found for these samples.[9] The decrease in PLLA concentration in the remaining solution during the crystallization process resulted from a change in the spherulite structure during growth, as demonstrated on an enlarged micrograph of the sample PLLA/DEET 10/90, shown in Figure 16. This is a characteristic of the spherulites obtained in samples containing 10, 20, and 30 wt.% PLLA. It is assumed the solution is relatively rich in PLLA macromolecules during the early stages of the nonisothermal crystallization process. This takes place at high temperatures, allowing the formation of relatively dense central parts within the spherulites, with a structure that may be like that of melt-crystallization, as shown in Figure 16. As the spherulites continue to grow, the solution's falling PLLA concentration and dropping temperature cause dendritic crystallization and frequent branching, which significantly reduces the concentration

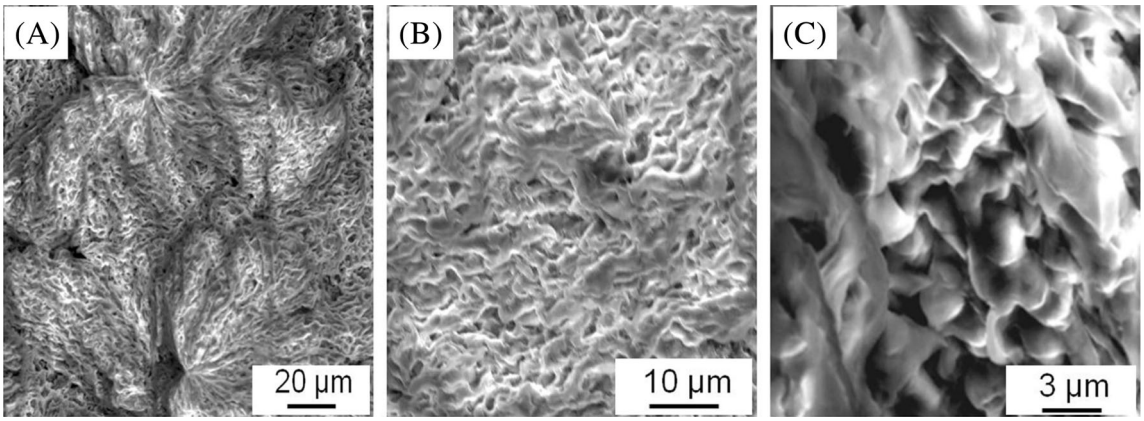

FIGURE 15 ESEM micrographs of PLLA/DEET system with 10 wt.% PLLA, after removal of the repellent using vacuum drying.[9] Adapted with permission from Elsevier Science Ltd.

and quantity of crystals per unit volume. Finally, growth stops if the content of PLLA macromolecules falls below a certain value or zero.[9]

In a novel approach that goes beyond earlier research on the utilization of various technologies to produce microporous PLA/DEET devices, the TIPS technique was utilized in 3D printing to fabricate the microporous PLLA-based IR3535.[112] The authors' first investigation into the field of polymer/repellent system 3D printing was in this study. Owing to its potential benefits, including increased productivity, multiple dosages and a complicated drug release profile, a single, low-cost process, and customization/personalization of drug delivery, 3D printing technology is widely used for pharmaceutical products and has drawn significant interest from both the drug industry and academia.[113,114] This updated technology is a very helpful tool for more accurate medication dispensing and customized drug release to meet each patient's specific needs. Furthermore, according to Mohapatra et al.,[114] personalized medicine presents an unparalleled chance for 3D printing to address the difficulties associated with treating a variety of diseases. Because it is inexpensive, 3D printing, a computerized technique, has significant uses in customized medicine dosage. According to published literature,[115–119] scaffolds with precisely controlled micro/nanostructures and designed shapes can be fabricated. As an alternative, 3D polymeric scaffolds ought to possess appropriate mechanical and biological characteristics along with hierarchical structures.[120–122] Fused deposition modeling (FDM), Polyjet, selective laser sintering, direct ink writing, stereolithography, and digital light processing are the main 3D printing technologies currently in use.[120] They can create scaffolds with linked macropore structures that are repeatable. Customized implants are made to precisely fit the patient's anatomical structure and the size of the defect.[82,122] Improving the mechanical qualities of scaffolds while preserving their proper porosity is the primary challenge of 3D printing.

Furthermore, products with less than 10 μm of microporosity are generally not printable with 3D printing.[116,123] In contrast, products with multiple microns of microporosity can be created using gas foaming. Multifunctional microporous scaffolds for drug delivery applications and bone tissue engineering can be prepared using this adaptable and hygienic method.[124–126] From the SEM analysis, the fabrication of intraspherulitic and interspherulitic pores, which acted as hosts of large amounts of repellent or a repellent-rich phase solution, was confirmed. Therefore, the effect of crystallization temperature on the structure of PLA samples initially containing 90 wt.% of IR3535 was investigated (Figure 17A). It was observed that the reduction of crystallization temperature affected the structures of PLA-based IR3535 samples, and this can be attributed to the number of spherulite growth.[112] In addition, the effect of concentration (10, 20, 30, and 40 wt.% of PLA) on the morphology of PLA and the crystallization temperature was evaluated (Figure 17B). For all the composition, the double distribution of cavities, interspherulitic and intraspherulitic, was clearly observed and visible.

Nevertheless, the SEM micrographs revealed that an increase in the concentration of polymer affected the intraspherulitic pore size. This means the size of the pores is reduced, seemingly deterring the solvent into interspherulitic areas to a larger level compared with compositions with low polymer contents. On examining a larger set of SEM micrographs, it appeared that the intraspherulitic pore size might be especially controlled by the concentration of polymer and temperature of crystallization. In addition, from these studies, numerous publications have documented the importance of PLA in

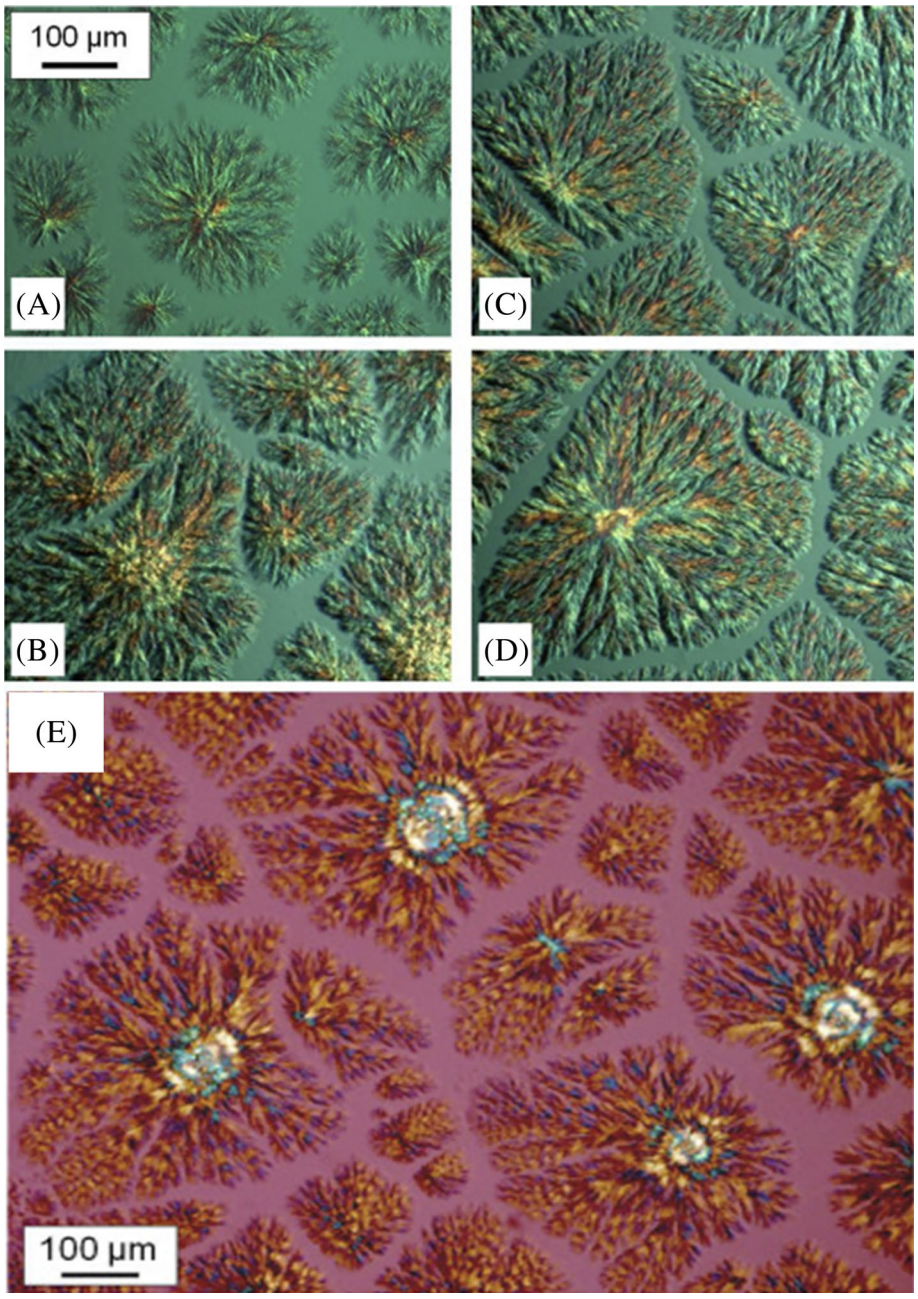

FIGURE 16 POM micrographs of slowly cooled of the PLLA/DEET system with 5 (A) 5 wt.%, (B) 10 wt.%, (C) 20 wt.%, (D) 30 wt.% of PLLA. (E) POM micrograph of a slowly cooled of the PLLA/DEET system with 10 wt.% PLLA was taken in transmission mode, using crossed polarizers and a λ-retardation plate.[9] Reproduced with permission from Elsevier Science Ltd.

the fabrication of microporous scaffolds for the biomedical field.[49,77,112,127,128]

It is evident from the SEM micrographs published in several publications[4,16,35,112] that the physical characteristics of the final microporous polymer membrane are largely determined by the concentration of polymer in the repellent system. The phase diagram indicates that when the concentration of the polymer is below the monotectic point (Figure 1), L–L phase separation and a cocontinuous polymer membrane morphology can be anticipated.[4] High permeability is demonstrated by the cocontinuous polymer membrane structure that was created using L–L phase separation.[15] Alternatively, if the polymer concentration is high enough to reach the monotectic phase, spherical polymer morphology formation will occur, which is driven by S–L phase separation. As a result, increasing the polymer concentration imposes stricter restrictions regarding the packing of spherulite structures and the polymer-lean phase, resulting in a tougher polymer membrane with denser surface structures (Figure 12D). On the other hand, a high concentration of polymers also raises the viscosity of the polymer/repellent system, which impacts the material's processability. When Mapossa et al.[96] prepared the PLA-based DEET/or IR3535 repellents using a melt-extrusion process, they noticed this behavior. Furthermore, the mechanical characteristics of the extruded polymer membranes were affected by the system's high polymer

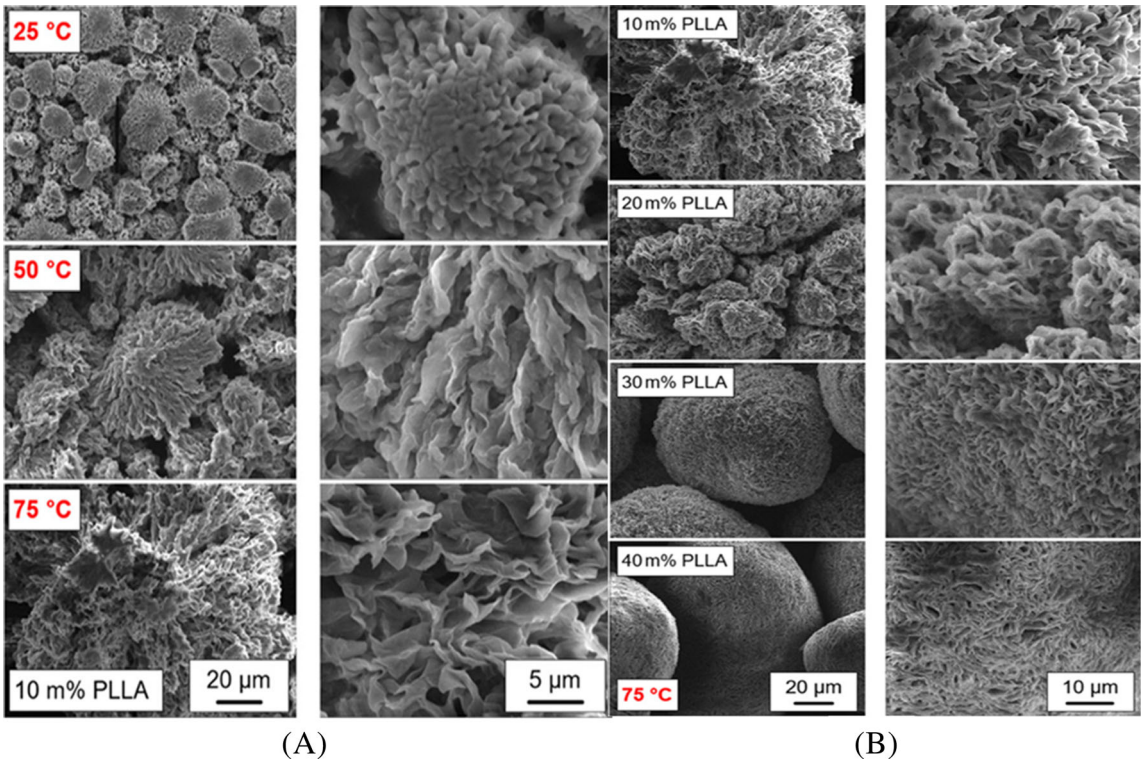

FIGURE 17 (A) SEM micrographs of the PLLA/IR3535 systems, primarily comprising 90 wt.% IR3535 crystallized at temperatures of 25, 50, and 75 °C. (B) SEM micrographs of the PLLA/IR3535 systems with 10, 20, 30, and 40 wt.% of PLLA crystallized at a temperature of 75 °C.[112] Reproduced with permission from ACS.

concentration.[15,129] In conclusion, it is critical to remember that numerous studies have demonstrated that liquid–liquid phase separation takes place when the polymer concentration falls below the monotectic point.[15] To enhance certain properties, such as mechanical properties, without temporarily changing the monotectic point, the authors advise increasing the polymer concentration to the maximum extent feasible.

In terms of the rate at which repellents were released from 3D-PLLA devices, the samples under investigation showed that at room temperature, the IR3535 was released from PLLA for a minimum of 10 days, irrespective of the initial concentration of repellent. The materials based on PLA/IR3535 will not work in tropical countries where malaria is endemic due to temperatures exceeding 45 °C, which makes the results inadequate. The biological activity of 3D-printed scaffolds is typically low, so surface modification technology is needed to increase it. Several techniques, including hyaluronic acid, collagen surface modification, surface peptide modification, and surface roughening, have been studied to address this issue.[122,130]

PBS is an aliphatic polyester produced from both fossil and renewable resources.[131] Furthermore, it is also produced via the polymerization of 1,4-butanediol with monomer succinic acid.[132,133] PBS is the most commercially competitive biodegradable polymer, which has increased its importance in several applications such as implants, packaging, or mulching films.[64,134–136] PBS has also been employed as an interesting polymeric material for the fabrication of scaffold structures for its application in bone tissue engineering.[113,137–140] The advantages of using PBS as a drug delivery system are that it can be easily prepared, extended, and controlled and can provide a consistent drug release. The polymer PBS is electrospun from solution to create nanofibers or emulsion polymerized to create microcapsules for use in biomedical applications.[141,142]

Till the year 2020, no study regarding the miscibility and demixing of the system PBS/DEET as a carrier for repellent for biomedical field applications had been explored. Therefore, studies regarding the use of PBS as a carrier of drug (i.e., repellent DEET) were first introduced by Yener et al.[64] The micro-/nano-porous biodegradable scaffolds suitable based on PBS devices for slow-release of insect repellent N, N-diethyl-3-methylbenzamide (DEET) was successfully prepared by TIPS method. SEM micrographs confirmed the microporous structure with interconnected pores or intraspherulitic features of the polymer. Spherulites ceased to be space-filling at higher crystallization temperatures of 30 and 60 °C due to the DEET-rich phase being positioned outside the spherulites.

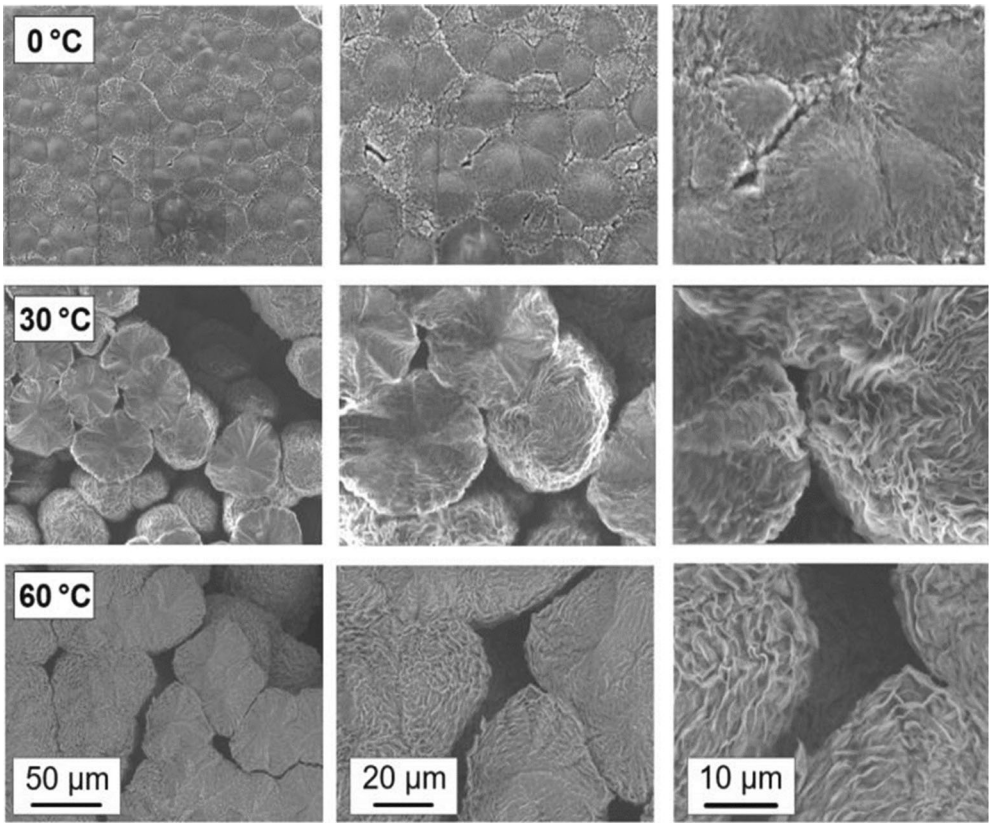

FIGURE 18 SEM micrographs of PBS/DEET systems with 30 wt.% PBS, crystallized temperatures of 0, 30, and 60 °C, obtained at various magnifications.[64] Reproduced with permission from Springer.

The right column's higher-resolution pictures in Figure 18 provided evidence regarding the solid intraspherulitic scaffold's structure obtained by lamellar PBS crystals. TIPS method at a temperature of 0 °C has led to a space-filled spherulitic morphology, that is, the DEET-rich phase (>70 wt.%) was filled into spherulites. The SEM micrographs formed at higher magnification (right side (10 μm) Figure 18) revealed intraspherulitic pores where DEET was hosted. In conclusion, it was noted that crystallization temperatures affected the structure of the PBS matrix. Additionally, from this study, additional works demonstrating the importance of PBS matrix in the formation of microporous structures for medical application have continued to be explored by the same researchers[65] and other groups of researchers.[143]

The impact of the polymer-diluent relationship (i.e., repellent) is important in TIPS technology. For example, choosing an appropriate diluent (repellent) is one of the main criteria for the TIPS technique. The right repellent should be low in molecular weight, high in boiling point, low in toxicity, and low impact on the environment, be inexpensive and be judiciously compatible with the polymer materials for a high range of temperatures and concentrations.[23]

Furthermore, the process of phase separation and the membrane morphology are significantly influenced by the good compatibility of the polymer and diluent, which has an impact on the microporous polymer membrane properties like pore size and distribution.[10,23] As a result of determining the polymer crystallization temperature of the mixture and the location of the binodal curve, for instance, the compatibility of the polymer and repellent form the system's phase diagram. With declining compatibility, the binodal curve swings to higher temperatures and vice-versa. Phase separation and, consequently, the shape and functionality of the microporous polymer membrane are influenced by the polymer-repellent interactions, as was covered in the preceding section. Consequently, L–L phase separation is caused by the repellent's low compatibility when used as a diluent with the polymer. However, the high repellent and polymer compatibility leads to S–L phase separation, which takes center stage in the system.[26,144,145] When dealing with binary systems, which consist of two diluents or repellents, it is critical to understand the differences between the two diluents, primary and secondary. A polymer should exhibit good compatibility with a primary diluent, while a secondary diluent should exhibit high compatibility with the primary diluent but less compatibility with the polymer.[43] A change from liquid–liquid phase separation to solid–liquid phase separation can be caused by the existence of a secondary diluent, which raises the polymer/diluent system's cloud point curve. Considering this, the polymer membrane's morphology gradually changes from spherulitic to continuous.[15,43,146]

The compatibility of polymer with diluents (i.e., repellents) can be estimated using Hansen's solubility parameter method. The parameters of the components of solubility are found in the literature and are applied to determine the total solubility of the parameters of the compounds according to Equation (14).[102]

$$\delta_T = \sqrt{\delta_D^2 + \delta_P^2 + \delta_H^2}, \quad (14)$$

where δ_D is dispersion, δ_P represents the polarity, and δ_H is a hydrogen bonding interaction.

Using Hansen's method, a roughly spherical solubility area can be transformed into a three-dimensional coordinate system, where the solubility parameters define the axes. The interaction radius (R_0) is the radius of this solubility sphere that is used to estimate the solubility of the polymer and diluent (i.e., repellent).[147] R_0 establishes the line that divides good diluents from bad diluents, with diluents inside the sphere having satisfactory compatibility with the polymer. People who are not in the sphere make bad solvents.[148] How well cellulose diacetate works as a repellent citronellol, terpineol, and methyl salicylate was described by[102] using Equation 15:

$$R_a = \left[4\left(\delta_{Ds} - \delta_{Dp}\right)^2 + \left(\delta_{Ps} - \delta_{Pp}\right)^2 + \left(\delta_{Hs} - \delta_{Hp}\right)^2\right]^{\frac{1}{2}}. \quad (15)$$

From Equation (15), good polymer–repellent compatibility is most possible when $R_a < R_0$, while the poor compatibility of polymer–repellent is then shown by $R_a > R_0$.[149,150]

As previously mentioned, the cooling rate is one of the key factors impacting the polymer–repellent system's crystallization and phase separation process during the TIPS technology. It is crucial to remember that various variables, such as altering different cooling rates, could be caused by the temperature of the coagulation solution, bore fluid, or quenching.[10] Different cooling conditions result in different times for phase separation and crystallization to develop because they are both induced by temperature change, which inevitably changes the membrane structure; for the system involving an L–L phase separation process, an enhanced cooling rate led to smaller pores because the polymer-lean crystals grew faster. A higher quenching temperature produces a spherulitic structure with a larger crystal size, more porosity, and lower tensile strength for a system that solely uses an S–L phase separation process.[10,151–153] Porous membranes have always had limited mechanical strength because of this. According to Gu et al. findings,[154] the membranes' high crystal potential and rapid cooling caused the crystallization to occur extremely quickly without coarsening.[154] The size of the spherulitic structure was measured at room temperature with a reasonably slow cooling and crystallization rate.

Additives can significantly alter the phase separation process, which in turn can alter the structure and activity of the polymer membrane. Despite the benefits associated with microporous polymer membranes (i.e., PE), which are highly hydrophobic and hence prone to catching, Some, such as PLLA, cannot be used in high-pressure systems due to their limited mechanical properties.[15] However, because they often take on noncontinuous morphologies, polymers like PLLA and PBS tend to result in membranes with undesired pore structures. Numerous additives, such as nucleation agents, macromolecule modifiers, and nonsolvent additives, have been added to the polymer membrane matrices to encourage a transition from S–L to L–L phase separation, increase membrane permeability, and increase mechanical resistance. In the diluted systems, certain additives are used to regulate the produced membranes' porous structure and separation performance, as previously mentioned (Figure 12). They are typically added for three different purposes, as illustrated in Figure 11, depending on their impact on the formation of the polymer membrane: to adjust pore formation, to support crystallization and growth by acting as nucleation sites, and to regulate nonsolvent inflow. The kinetics and thermodynamics of diluent-rich droplet growth can also be influenced by additives in the first group, which can change the equilibrium between L–L and S–L phase separation.[15]

5 | CONCLUSION AND OUTLOOK CHALLENGES

This review presents the recent trends and challenges for the emerging materials class of microporous polymers as devices of insect repellents produced by TIPS methods. The topics described in this article are certainly chosen in a highly subjective manner; however, the authors tried to focus mainly on crystallization behavior and morphological studies of polymeric membrane materials-based repellents performed by DSC, SEM, and POM techniques. Several studies have confirmed that semi-crystalline morphologies are qualitatively different from morphologies obtained after crystallization at high temperatures, affecting properties. For many different polymers, crystallization at low temperatures frequently proceeds by homogeneous crystal nucleation. It is important to note that the effect of repellent type and type of polymer, amount of repellent and polymer, as well as the additive (filler), have affected the crystallization behavior and morphology of the polymer/repellent systems. However, the possibility of producing repellent-processable microporous polymers or

generating extruded polymeric materials containing repellent via the TIPS method to be used for long periods as a reservoir for large amounts of repellent in medical applications makes microporous polymers an exciting field for further research. With all the options at hand, it is anticipated that more membrane technology applications will be made possible by the development of porous polymeric membranes with excellent permeability, good stability, and well-controlled morphology.

These scientists worked on creating a polymer product that traps more repellents into a polymer device, serving as a reservoir for those appropriate repellents. A blooming mechanism may then be used to release the active ingredient. A disadvantage of this method, nevertheless, would be an exponential decay of the release rate over time, primarily being high but later, when needed, being insufficient. The limited solubility of the liquid active in the polymer matrix and swelling of the polymer if the repellent dissolves in the matrix present another difficulty for this strategy. In the latter case, the product's dimensional stability will be impacted as the polymer gradually shrinks as the active ingredient is released. Another challenge is the price, which remains the main concern for biodegradable polymer implementation. This has resulted in delayed legislation due to push back from increasing consumer goods prices in the future. Additional investigations, which include the thermodynamic aspects and microporous polymer membrane fabrication procedure, are required to make controllable microporous polymer membrane preparation with improved performance.

Additionally, the microporous polymer membrane fabrication procedure is vital in improving the membrane structure; a minor adjustment can affect the positivity of the membrane performance. In the next studies, scientists can also focus on developing new techniques to realize development and industrialization, which would also comply with the research routine offered by this work. Therefore, this article would be a useful reference for investigators focusing on the manufacturing and development of microporous polymeric membranes as devices for drug delivery using TIPS technology.

Although works are reporting the thermodynamic aspects, particularly Floy–Huggin's theory for polymer/repellent phase systems with successful results, in the future, to realize controllable the formation of the membrane with superior performance, fundamental evolution will emerge both in the thermodynamic research and membrane formation procedure. For the thermodynamic aspect, although at least three criteria introduced in this manuscript can be followed to find new repellent (diluent) systems, researchers occasionally feel confused because of the lack of basic physical parameters.

ACKNOWLEDGMENTS

The authors thank the Natural Sciences and Engineering Research Council of Canada (NSERC) Discovery Grant (05503/2020), and Department of Science and Innovation, South Africa, for funding support and the Department of Chemical, Metallurgical and Materials, Tshwane University of Technology, South Africa, for all technical and logistical support. SSR would like to acknowledge financial support from the Nanotechnology Innovation Centre (C6ACH77), South Africa and Council for Scientific and Industrial Research (C6A0059).

CONFLICT OF INTEREST STATEMENT

The authors declare no conflict of interest.

ORCID

António Benjamim Mapossa https://orcid.org/0000-0003-3824-5356
Robert Kimutai Tewo https://orcid.org/0000-0002-2739-202X
Suprakas Sinha Ray https://orcid.org/0000-0002-0007-2595
Washington Mhike https://orcid.org/0000-0003-4670-1171
Uttandaraman Sundararaj https://orcid.org/0000-0003-4124-3917

REFERENCES

[1] P. M. Budd, S. M. Makhseed, B. S. Ghanem, K. J. Msayib, C. E. Tattershall, N. B. McKeown, *Mater. Today* **2004**, *7*, 40.
[2] X. Zou, G. Zhu, *Microporous Materials for Separation Membranes*, Wiley-VCH Verlag GmbH & Co. KGaA, Weinheim **2019**.
[3] A. Figoli, *Encyclopedia of Membranes*, Springer, Berlin, Heidelberg **2015**.
[4] A. B. Mapossa, M. M. Sibanda, A. Sitoe, W. W. Focke, L. Braack, C. Ndonyane, J. Mouatcho, J. Smart, H. Muaimbo, R. Androsch, M. T. Loots, *Chem. Eng. J.* **2019**, *360*, 435.
[5] A. B. Mapossa, A. Sitoe, W. W. Focke, H. Izadi, E. L. du Toit, R. Androsch, C. Sungkapreecha, E. M. van der Merwe, *Pest Manage. Sci.* **2020**, *76*, 1112.
[6] D. R. Lloyd, *J. Membr. Sci.* **1990**, *52*, 239.
[7] J. Kim, J. H. Kim, Y. Lee, *Adv. Mater. Sep. Mater. Devices Process. J* **2012**, *59*, 215.
[8] M. Liu, S. Liu, Z. Xu, Y. Wei, H. Yang, *Front. Chem. Sci. Eng.* **2016**, *10*, 57.
[9] C. Sungkapreecha, N. Iqbal, A. M. Gohn, W. W. Focke, R. Androsch, *Polymer* **2017**, *126*, 116.
[10] Y. Tang, Y. Lin, W. Ma, X. Wang, *J. Membr. Sci.* **2021**, *639*, 119759.
[11] L. Sheng, Y. Du, H. Zhang, Z. Chen, J. Pan, T. Wang, X. Huang, J. He, *Polym. Bull.* **2020**, *77*, 165.
[12] A. Laxminarayan, K. S. McGuire, S. S. Kim, D. R. Lloyd, *Polymer* **1994**, *35*, 3060.
[13] P. Vandeweerdt, H. Berghmans, Y. Tervoort, *Macromolecules* **1991**, *24*, 3547.
[14] P. van de Witte, A. Boorsma, H. Esselbrugge, P. J. Dijkstra, J. W. A. van den Berg, J. Feijen, *Macromolecules* **1996**, *29*, 212.

[15] W. Ma, Z. Zhou, N. Ismail, E. Tocci, A. Figoli, M. Khayet, T. Matsuura, Z. Cui, N. Tavajohi, *J. Membr. Sci.* **2023**, *669*, 121303.
[16] K. Phala, A. B. Mapossa, W. Augustyn, S. Combrinck, B. Botha, *Arabian J. Chem.* **2023**, *16*, 104458.
[17] A. B. Mapossa, A. H. da Silva Júnior, W. Mhike, U. Sundararaj, C. R. Silva de Oliveira, *Macromol. Mater. Eng.* **2024**, *309*, 2400130.
[18] B. Díez, R. Rosal, *Nanotechnol. Environ. Eng.* **2020**, *5*, 1.
[19] S. Kim, Y. M. Lee, *Prog. Polym. Sci.* **2015**, *43*, 1.
[20] E. Rezabeigi, P. M. Wood-Adams, N. R. Demarquette, *Macromolecules* **2018**, *51*, 4094.
[21] X. Du, S. Fu, Y. Zhu, *J. Mater. Chem. B* **2018**, *6*, 4397.
[22] A. M. Ziemba, K. P. Lane, I. M. San Segundo, A. R. D'Amato, A. K. Mason, R. J. Sexton, H. Casajus, R. A. Gross, D. T. Corr, R. J. Gilbert, *ACS Biomater. Sci. Eng.* **2018**, *4*, 1491.
[23] J. T. Jung, J. F. Kim, H. H. Wang, E. di Nicolo, E. Drioli, Y. M. Lee, *J. Membr. Sci.* **2016**, *514*, 250.
[24] D. J. Hellman, A. R. Greenberg, W. B. Krantz, *J. Membr. Sci.* **2004**, *230*, 99.
[25] S. Liu, C. Zhou, W. Yu, *J. Membr. Sci.* **2011**, *379*, 268.
[26] B. J. Cha, K. Char, J. J. Kim, S. S. Kim, C. K. Kim, *J. Membr. Sci.* **1995**, *108*, 219.
[27] J. L. Shi, L. F. Fang, H. Zhang, Z. Y. Liang, B. K. Zhu, L. P. Zhu, *J. Appl. Polym. Sci.* **2013**, *130*, 2680.
[28] D. R. Lloyd, S. S. Kim, K. E. Kinzer, *J. Membr. Sci.* **1991**, *64*, 1.
[29] Z. Yang, P. Li, L. Xie, Z. Wang, S. C. Wang, *Desalination* **2006**, *192*, 168.
[30] X. Li, C. Chen, J. Li, *J. Membr. Sci.* **2008**, *314*, 206.
[31] S. Rajabzadeh, S. Yoshimoto, M. Teramoto, M. Al-Marzouqi, H. Matsuyama, *Sep. Purif. Technol.* **2009**, *69*, 210.
[32] J. Zhou, H. Zhang, H. Wang, Q. Du, *J. Membr. Sci.* **2009**, *343*, 104.
[33] H. Matsuyama, H. Yano, T. Maki, M. Teramoto, K. Mishima, K. Matsuyama, *J. Membr. Sci.* **2001**, *194*, 157.
[34] J. K. Kim, K. Taki, M. Ohshima, *Langmuir* **2007**, *23*, 12397.
[35] M. U. Akhtar, W. W. Focke, *Thermochim. Acta* **2015**, *613*, 61.
[36] H. Matsuyama, H. Okafuji, T. Maki, M. Teramoto, N. Kubota, *J. Membr. Sci.* **2003**, *223*, 119.
[37] L. Shen, M. Peng, F. Qiao, J. L. Zhang, *Chin. J. Polym. Sci.* **2008**, *26*, 653.
[38] X. Wang, R. Wang, C. Peng, H. Li, *Prog. Nat. Sci.: Mater. Int.* **2012**, *22*, 347.
[39] I. Nascimento, R. E. Bruns, D. F. Siqueira, S. P. Nunes, *J. Brazilian Chem. Soc.* **1997**, *8*, 587.
[40] H. Matsuyama, S. Berghmans, M. T. Batarseh, D. R. Lloyd, *J. Membr. Sci.* **1998**, *142*, 27.
[41] M. Müller, V. Abetz, *Chem. Rev.* **2021**, *121*, 14189.
[42] C. Kahrs, J. Schwellenbach, *Polymer* **2020**, *186*, 122071.
[43] B. Zhou, Q. Li, Y. Tang, Y. Lin, X. Wang, *Desalin. Water Treat.* **2016**, *57*, 17646.
[44] B. F. Barton, A. J. McHugh, *J. Polym. Sci. Part B: Polym. Phys.* **1999**, *37*, 1449.
[45] H. Manzanarez, J. P. Mericq, P. Guenoun, J. Chikina, D. Bouyer, *Chem. Eng. Sci.* **2017**, *173*, 411.
[46] A. Venault, Y. Chang, D.-M. Wang, D. Bouyer, *Polym. Rev.* **2013**, *53*, 568.
[47] N. Metropolis, A. W. Rosenbluth, M. N. Rosenbluth, A. H. Teller, E. Teller, *J. Chem. Phys.* **1953**, *21*, 1087.
[48] Y. Fu, L. Liao, L. Yang, Y. Lan, L. Mei, Y. Liu, S. Hu, *Mol. Simul.* **2013**, *39*, 415.
[49] C. Sungkapreecha, M. J. Beily, J. Kressler, W. W. Focke, R. Androsch, *Thermochim. Acta* **2018**, *660*, 77.
[50] P. J. Flory, *J. Chem. Phys.* **1942**, *10*, 51.
[51] M. L. Huggins, *J. Chem. Phys.* **1941**, *9*, 440.
[52] K. S. McGuire, A. Laxminarayan, D. R. Lloyd, *Polymer* **1994**, *35*, 4404.
[53] J. Arnauts, R. De Cooman, P. Vandeweerdt, R. Koningsveld, H. Berghmans, *Thermochim. Acta* **1994**, *238*, 1.
[54] A. Toda, R. Androsch, C. Schick, *Polymer (Guildf).* **2016**, *91*, 239.
[55] health_and_disease_modeling_application_instructions (1).pdf.
[56] G. B. A. Lim, K. S. McGuire, D. R. Lloyd, *Polym. Eng. Sci.* **1993**, *33*, 537.
[57] S. Quattrosoldi, R. Androsch, A. Janke, M. Soccio, N. Lotti, *Polymer* **2020**, *12*, 235.
[58] R. Androsch, C. Schick, M. L. di Lorenzo, *Adv. Polym. Sci.* **2018**, *279*, 235.
[59] G. Strobl, *The Physics of Polymers: Concepts for Understanding Their Structures and Behavior*, Springer, Berlin **2007**.
[60] T. Miyata, T. Masuko, *Polymer* **1998**, *39*, 1399.
[61] G. Z. Papageorgiou, D. N. Bikiaris, *Polymer* **2005**, *46*, 12081.
[62] Z. Gan, H. Abe, H. Kurokawa, Y. Doi, *Biomacromolecules* **2001**, *2*, 605.
[63] E. S. Yoo, S. S. Im, *J. Polym. Sci. Part B: Polym. Phys.* **1999**, *37*, 1357.
[64] H. E. Yener, G. Hillrichs, R. Androsch, *Colloid Polym. Sci.* **2021**, *299*, 873.
[65] H. E. Yener, R. Erdmann, K. Jariyavidyanont, A. B. Mapossa, W. W. Focke, G. Hillrichs, R. Androsch, *ACS Omega* **2022**, *7*, 8377.
[66] X. Wang, J. Zhou, L. Li, *Eur. Polym. J.* **2007**, *43*, 3163.
[67] H. Zhang, J. Zhou, X. Zhang, H. Wang, W. Zhong, Q. Du, *Eur. Polym. J.* **2008**, *44*, 1095.
[68] K. J. Ihn, E. S. Yoo, S. S. Im, *Macromolecules* **1995**, *28*, 19.
[69] Q. Yu, A. Anuar, A. Petzold, J. Balko, K. Saalwächter, T. Thurn-Albrecht, *Macromol. Chem. Phys.* **2023**, *224*, 1.
[70] J. W. Park, D. K. Kim, S. S. Im, *Polym. Int.* **2002**, *51*, 239.
[71] T. Fujimaki, *Polym. Degrad. Stab.* **1998**, *59*, 209.
[72] J. E. K. Schawe, *J. Therm. Anal. Calorim.* **2014**, *116*, 1165.
[73] K. Jariyavidyanont, J. L. Williams, A. M. Rhoades, I. Kühnert, W. Focke, R. Androsch, *Polym. Eng. Sci.* **2017**, *4*, 1.
[74] E. Martuscelli, *Polym. Eng. Sci.* **1984**, *24*, 563.
[75] I. C. Sanchez, R. K. Eby, *Macromolecules* **1975**, *8*, 638.
[76] P. J. Flory, *J. Chem. Phys.* **1949**, *17*, 223.
[77] C. Sungkapreecha, N. Iqbal, W. W. Focke, R. Androsch, *Polym. Cryst.* **2019**, *2*, p.e10029.
[78] V. Maquet, R. Jerome, *Mater. Sci. Forum* **1997**, *250*, 15.
[79] D. W. Hutmacher, *Biomater. Silver Jubil. Compend.* **2000**, *21*, 175.
[80] D. Wu, J. Zhang, W. Zhou, Z. Yao, M. Zhang, D. Lin, J. Wang, *Polym. Int.* **2014**, *63*, 470.
[81] X. M. Tan, D. Rodrigue, *Polymer* **2019**, *11*, 1160.
[82] M. A. Heinrich, W. Liu, A. Jimenez, J. Yang, A. Akpek, X. Liu, Q. Pi, X. Mu, N. Hu, R. M. Schiffelers, J. Prakash, J. Xie, Y. S. Zhang, *Small* **2019**, *15*, e1805510.
[83] H. Matsuyama, M. man Kim, D. R. Lloyd, *J. Membr. Sci.* **2002**, *204*, 413.
[84] M. Zhang, C. F. Zhang, Z. K. Yao, J. L. Shi, B. K. Zhu, Y. Y. Xu, *Chin. J. Polym. Sci.* **2010**, *28*, 337.
[85] C. Zhang, Y. Bai, Y. Sun, J. Gu, Y. Xu, *J. Membr. Sci.* **2010**, *365*, 216.
[86] H. Ding, Y. Tian, L. Wang, B. Liu, *J. Appl. Polym. Sci.* **2010**, *116*, 2658.
[87] H. Sun, K. B. Rhee, T. Kitano, S. I. Mah, *J. Appl. Polym. Sci.* **2000**, *75*, 1235.

[88] C. J. Sahle, M. Zschintzsch, C. Sternemann, J. von Borany, A. Mücklich, A. Nyrow, N. M. Jeutter, R. Wagner, R. Frahm, M. Tolan, *Nanotechnology* **2011**, *22*, p.125709.

[89] Z. H. Rao, G. Q. Zhang, *Energy Sources, Part A* **2011**, *33*, 587.

[90] J. L. Shi, L. F. Fang, H. Zhang, Z. Y. Liang, B. K. Zhu, L. P. Zhu, *J. Appl. Polym. Sci.* **2013**, *130*, 3816.

[91] H. Sun, K. B. Rhee, T. Kitano, S. I. Mah, *J. Appl. Polym. Sci.* **1999**, *73*, 2135.

[92] S. S. Fu, H. Mastuyama, M. Teramoto, *Sep. Purif. Technol.* **2004**, *36*, 17.

[93] M. J. Park, S. C. Noh, C. K. Kim, *Ind. Eng. Chem. Res.* **2013**, *52*, 10690.

[94] D. W. Lee, C. M. Jensen, *J. Chem. Educ.* **2000**, *77*, 629.

[95] A. Sitoe, A. B. Mapossa, W. W. Focke, H. Muiambo, R. Androsch, J. Wesley-Smith, *SPE Polym.* **2020**, *1*, 90.

[96] A. B. Mapossa, W. W. Focke, R. K. Tewo, R. Androsch, T. Kruger, *Malar. J.* **2021**, *20*, 165.

[97] E. Ugel, G. Giuliano, M. Modesti, *Soft Nanosci. Lett.* **2011**, *1*, 105.

[98] C. Fang, S. Rajabzadeh, P. Zhang, W. Liu, N. Kato, H. K. Shon, H. Matsuyama, *J. Membr. Sci.* **2020**, *609*, 118229.

[99] Y. X. Bai, J. W. Qian, Q. Zhao, Z. H. Zhu, P. Zhang, *J. Membr. Sci.* **2007**, *299*, 45.

[100] K. Sadeghi, *GAU J. Soc. Appl. Sci* **2008**, *4*, 67.

[101] S. M. Willerth, S. E. Sakiyama-Elbert, *Adv. Drug Delivery Rev.* **2007**, *59*, 325.

[102] T. N. Mphateng, A. B. Mapossa, J. Wesley-Smith, S. Ramjee, W. W. Focke, *Cellulose* **2022**, *29*, 3915.

[103] Y. S. Nam, T. G. Park, *J. Biomed. Mater. Res.* **1999**, *47*, 8.

[104] F. J. Hua, G. E. Kim, J. D. Lee, Y. K. Son, D. S. Lee, *J. Biomed. Mater. Res.* **2002**, *63*, 161.

[105] F. Yang, R. Murugan, S. Ramakrishna, X. Wang, Y. X. Ma, S. Wang, *Biomaterials* **2004**, *25*, 1891.

[106] Ö. C. Önder, E. Yilgör, I. Yilgör, *Polymer* **2016**, *107*, 240.

[107] Y. Zhang, X. Zhao, X. Zhang, S. Peng, *Water Sci. Technol. Water Supply* **2015**, *15*, 442.

[108] D. Garlotta, *J. Polym. Environ.* **2001**, *9*, 63.

[109] R. Auras, B. Harte, S. Selke, *Macromol. Biosci.* **2004**, *4*, 835.

[110] H. Urayama, S. Il Moon, Y. Kimura, *Macromol. Mater. Eng.* **2003**, *288*, 137.

[111] E. Rezabeigi, P. M. Wood-Adams, R. A. L. Drew, *Polymer* **2014**, *55*, 3100.

[112] F. Du, R. Erdmann, A. Petzold, A. Wutzler, A. Leuteritz, M. Nase, R. Androsch, *Pharmaceutics* **2022**, *14*, 2381.

[113] J. Ju, Z. Gu, X. Liu, S. Zhang, X. Peng, T. Kuang, *Int. J. Biol. Macromol.* **2020**, *147*, 1164.

[114] S. Mohapatra, R. K. Kar, P. K. Biswal, S. Bindhani, *Sensors Int.* **2022**, *3*, 100146.

[115] S. Lee, M. K. Joshi, A. P. Tiwari, B. Maharjan, K. S. Kim, Y. H. Yun, C. H. Park, C. S. Kim, *Chem. Eng. J.* **2018**, *347*, 771.

[116] P. Song, C. Zhou, H. Fan, B. Zhang, X. Pei, Y. Fan, Q. Jiang, R. Bao, Q. Yang, Z. Dong, X. Zhang, *Composites, Part B* **2018**, *152*, 151.

[117] M. M. Kareem, T. Hodgkinson, M. S. Sanchez, M. J. Dalby, K. E. Tanner, *Biomed. Mater.* **2019**, *14*, 25008.

[118] B. I. Oladapo, S. A. Zahedi, A. O. M. Adeoye, *Composites, Part B* **2019**, *158*, 428.

[119] L. Zhao, X. Pei, L. Jiang, C. Hu, J. Sun, F. Xing, C. Zhou, Y. Fan, X. Zhang, *Composites, Part B* **2019**, *162*, 154.

[120] X. Dai, X. Li, M. Zhang, J. Xie, X. Wang, *ACS Omega* **2018**, *3*, 6860.

[121] J. P. A. Freitas, F. R. M. França, M. S. Silva, R. J. Toms, G. F. da Silva, *Brazilian J. Chem. Eng.* **2019**, *36*, 905.

[122] L. R. Jaidev, K. Chatterjee, *Mater. Des.* **2019**, *161*, 44.

[123] J. Babilotte, V. Guduric, D. le Nihouannen, A. Naveau, J. C. Fricain, S. Catros, *J. Biomed. Mater. Res., Part B* **2019**, *107*, 2579.

[124] D. Maniglio, W. Bonani, C. Migliaresi, A. Motta, *J. Biomater. Sci., Polym. Ed.* **2018**, *29*, 491.

[125] M. Costantini, A. Barbetta, *Gas Foaming Technologies for 3D Scaffold Engineering*, Elsevier Ltd, Amsterdam **2018**.

[126] X. Xin, Y. X. Guan, S. J. Yao, *J. Appl. Polym. Sci.* **2018**, *135*, 23.

[127] F. Du, C. Schick, R. Androsch, *Polymer* **2020**, *209*, 123058.

[128] C. Sungkapreecha, W. W. Focke, R. Androsch, *Chin. J. Polym. Sci.* **2020**, *38*, 174.

[129] I. Ferreira, H. Brünig, W. Focke, R. Boldt, R. Androsch, A. Leuteritz, *Materials* **2021**, *14*, 1.

[130] A. Coolen, C. Lacroix, P. Mercier-gouy, E. Delaune, C. Monge, J. Exposito, B. Verrier, A. Coolen, C. Lacroix, P. Mercier-gouy, E. Delaune, C. Monge, *Biomaterials* **2021**, *195*, 23.

[131] Y. Zhang, S. Zhou, X. Fang, X. Zhou, J. Wang, F. Bai, S. Peng, *Eur. Polym. J.* **2019**, *116*, 265.

[132] L. Song, Z. Qiu, *Polym. Degrad. Stab.* **2009**, *94*, 632.

[133] N. Karakehya, *Int. J. Adhes. Adhes.* **2021**, *110*, 102949.

[134] J. Xu, B. H. Guo, *Biotechnol. J.* **2010**, *5*, 1149.

[135] J. Xu, B.H. Guo, Microbial Succinic Acid. Its Polymer Poly (butylene succinate), and Applications, *Plastics from Bacteria, Springer Berlin Heidelberg*, **2010**, *14*, 347.

[136] V. Siracusa, N. Lotti, A. Munari, M. Dalla Rosa, *Polym. Degrad. Stab.* **2015**, *119*, 35.

[137] F. Cristofaro, M. Gigli, N. Bloise, H. Chen, G. Bruni, A. Munari, L. Moroni, N. Lotti, L. Visai, *Nanoscale* **2018**, *10*, 8689.

[138] Z. Wu, K. Zheng, J. Zhang, T. Tang, H. Guo, A. R. Boccaccini, J. Wei, *J. Mater. Chem. B* **2016**, *4*, 7974.

[139] M. Gigli, M. Fabbri, N. Lotti, R. Gamberini, B. Rimini, A. Munari, *Eur. Polym. J.* **2016**, *75*, 431.

[140] D. Zhang, J. Chang, Y. Zeng, *J. Mater. Sci.: Mater. Med.* **2008**, *19*, 443.

[141] C. T. Brunner, E. T. Baran, E. D. Pinho, R. L. Reis, N. M. Neves, *Colloids Surf., B* **2011**, *84*, 498.

[142] A. Sonseca, R. Sahay, K. Stepien, J. Bukala, A. Wcislek, A. McClain, P. Sobolewski, X. M. Sui, J. E. Puskas, J. Kohn, H. D. Wagner, M. El Fray, *Mater. Sci. Eng. C* **2020**, *108*, 110505.

[143] R. Zeinali, L. Franco, L. J. del Valle, J. Puiggalí, *Polymer* **2022**, *252*, 124916.

[144] Y. Su, C. Chen, Y. Li, J. Li, *J. Macromol. Sci., Part A: Pure Appl.Chem.* **2007**, *44*, 305.

[145] M. Conti, U. M. B. Marconi, *Phys. A (Amsterdam, Neth.)* **2000**, *280*, 148.

[146] C. Ursino, I. Ounifi, E. Di Nicolò, X. Q. Cheng, L. Shao, Y. Zhang, E. Drioli, A. Criscuoli, A. Figoli, *Desalination* **2021**, *500*, 114879.

[147] J. Stephen, B. Ghorani, S. J. Russell, P. Goswami, *Hindawi* **2013**, *2013*, p.256161.

[148] M. J. M. Wells, A. Morse, K. Y. Bell, M.-L. Pellegrin, L. J. Fono, *Emerging Pollut.* **2009**, *81*, 2211.

[149] M. T. García, I. Gracia, G. Duque, A. de Lucas, J. F. Rodríguez, *Waste Manage.* **1814**, *2009*, 29.

[150] S. I. Swapnil, N. Datta, M. M. Mahmud, R. A. Jahan, M. T. Arafat, *J. Appl. Polym. Sci.* **2021**, *138*, 1.

[151] K. Nakatsuka, Y. Ohmukai, T. Maruyama, H. Matsuyama, *Desalin. Water Treat.* **2010**, *17*, 275.
[152] N. T. Hassankiadeh, Z. Cui, J. H. Kim, D. W. Shin, A. Sanguineti, V. Arcella, Y. M. Lee, E. Drioli, *J. Membr. Sci.* **2014**, *471*, 237.
[153] Z. Yang, H. Peng, W. Wang, T. Liu, *J. Appl. Polym. Sci.* **2010**, *116*, 2658.
[154] M. Gu, J. Zhang, X. Wang, H. Tao, L. Ge, *Desalination* **2006**, *192*, 160.

AUTHOR BIOGRAPHIES

Dr. **António Benjamim Mapossa** obtained his PhD degree from the Department of Chemical Engineering, University of Pretoria, South Africa, where he also worked a postdoctoral researcher. Currently, he is a researcher associate in the Department of Chemical and Petroleum Engineering, University of Calgary, Canada. His research focus is primarily centered on Materials Science and Engineering with a special focus on the structure, processing, and properties of polymer nanocomposites and nanomagnetic materials toward malaria, agriculture, flooring materials, biodiesel, and water and wastewater applications. He is a Y2-rated researcher as benchmarked by the South African National Research Foundation recognized by peers in his field.

Dr. **Robert Kimutai Tewo** obtained his PhD degree from the Department of Chemical Engineering, University of Pretoria, South Africa. He is a Lecturer in the Department of Chemical Engineering at Dedan Kimathi University of Technology, Kenya. His research focuses on polymer technology and materials engineering.

Prof. **Suprakas Sinha Ray** is a chief researcher in Nanoscience and Nanotechnology at the Council for Scientific and Industrial Research (CSIR), Pretoria, South Africa. He was awarded a PhD in physical chemistry by the University of Calcutta in 2001 and is director of the DSI-CSIR, Nanotechnology Innovation Centre, and manager of the Centre for Nanostructures and Advanced Materials. He is also affiliated with the University of Johannesburg as a distinguished professor of chemistry. Prof. Ray's current research focus is on polymer-based advanced nanostructured materials and their applications.

Dr **Washington Mhike** obtained his PhD from the Department of Chemical Engineering, University of Pretoria in 2016. He is a lecturer in the Department of Chemical, Metallurgical, and Materials Engineering at the Tshwane University of Technology, Pretoria. His research is focused on solving prevailing societal problems through applied materials research. He is presently working on the development of "next generation" long lasting insecticide treated mosquito nets for the prevention of malaria, among other research areas which include applications of polymeric materials in water treatment, development of cost effective compostable medical devices, and development of "green" flame retardant additives for polymers.

Prof. **Uttandaraman Sundararaj** joined the University of Calgary in August 2009. Previously he was Professor at University of Alberta for 12 years. He has 4 years of industrial experience with General Electric Company—Plastics Division. He was Visiting Professor at University of California—Santa Barbara, University of Paderborn (Germany), Institute for Polymer Research—Dresden (Germany), and at Dupont Experimental Station—Delaware.

How to cite this article: A. B. Mapossa, R. K. Tewo, S. S. Ray, W. Mhike, U. Sundararaj, *J. Polym. Sci.* **2024**, 1. https://doi.org/10.1002/pol.20240232